

AD-A071 480

GEORGE WASHINGTON UNIV WASHINGTON D C SCHOOL OF ENGI--ETC F/G 20/11
LARGE DEFORMATION ELASTIC-PLASTIC BUCKLING ANALYSIS OF SPHERICA--ETC(U)
MAY 79 R KAO

N00014-75-C-0946

NL

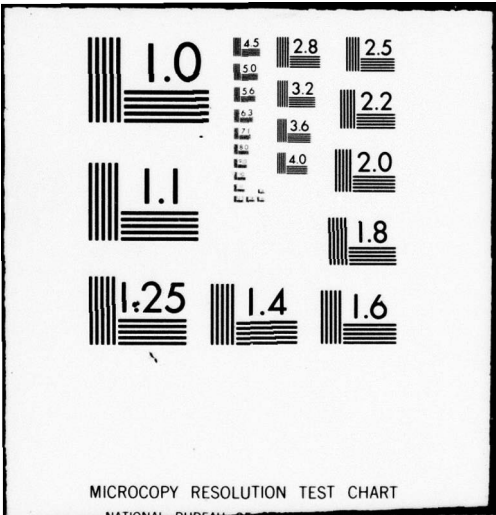
UNCLASSIFIED

1 OF 1

ADA
071480



END
DATE
FILMED
8-79
DDC



LEVEL II



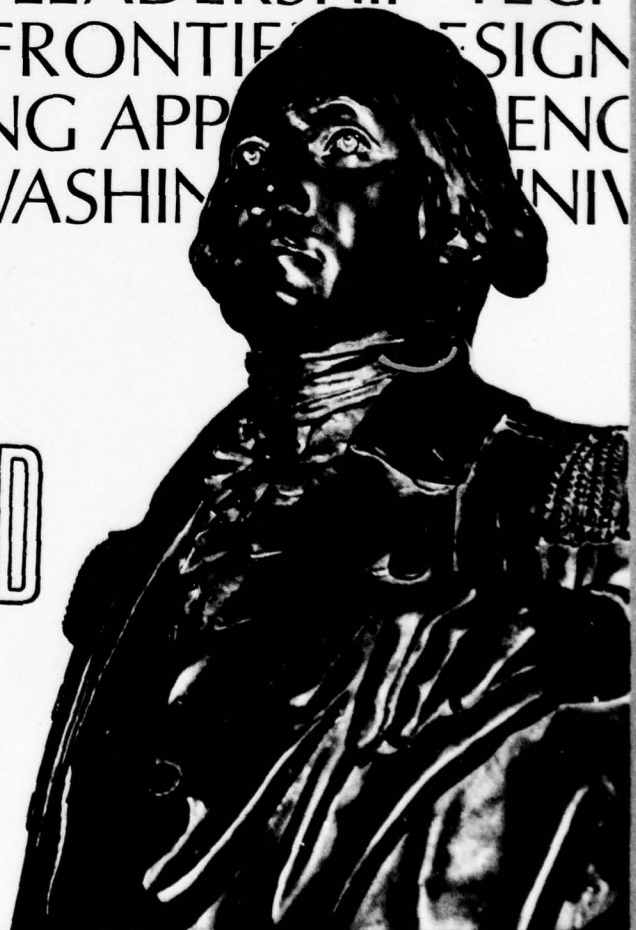
DA071480

THE
GEORGE
WASHINGTON
UNIVERSITY

STUDENTS FACULTY STUDY R
ESEARCH DEVELOPMENT FUT
URE CAREER CREATIVITY CO
MMUNITY LEADERSHIP TECH
NOLOGY FRONTIER DESIGN
ENGINEERING APP ENC
GEORGE WASHINGTON UNIV

DDC FILE COPY.

DDC
RECEIVED
JUL 23 1979
REGISTRY
D



79 07

19 004

SCHOOL OF ENGINEERING
AND APPLIED SCIENCE

Accession For	
NTIS GRA&I	<input checked="" type="checkbox"/>
DDC TAB	<input type="checkbox"/>
Unannounced	<input type="checkbox"/>
Justification	
By _____	
Distribution/	
Availability Codes	
Dist.	Avail and/or special
A	

LEVEL II

⑥
LARGE DEFORMATION ELASTIC-PLASTIC
BUCKLING ANALYSIS OF SPHERICAL CAPS
WITH INITIAL IMPERFECTIONS.

⑩ Robert/Kao

⑮ N00014-75-C-0946

Sponsored by
 Office of Naval Research
 Arlington, Virginia 22217

Contract Number
 NAVY 00014-75-C-0946

⑫ 52a

⑪ May 1979

DISTRIBUTION STATEMENT A
 Approved for public release;
 Distribution Unlimited

School of Engineering and Applied Science
 The George Washington University
 Washington, D.C. 20052

DDC
 RECEIVED
 JUL 23 1979
 D

153 370 79 07 19 004

JOB

LARGE DEFORMATION ELASTIC-PLASTIC BUCKLING ANALYSIS OF
SPHERICAL CAPS WITH INITIAL IMPERFECTIONS¹

by
Robert Kao

¹ The research reported on here was supported by the Office
of Naval Research, Contract Number NAVY 00014-75-C-0946

ABSTRACT

Large deformation elastic-plastic buckling loads are obtained for axisymmetric spherical caps with initial imperfections. The problem formulation is based on equilibrium equations in which the plastic deformation is taken as an effective plastic load. Both perfectly plastic and strain hardening behavior are considered. Strain hardening is represented by the Prager-Ziegler kinematic hardening theory, so that the Bauschinger effect is accounted for. Solutions of elastic-plastic circular plates and spherical caps are in good agreement with previous results. For the spherical cap it was determined that both initial imperfection and plastic deformation have the same effect of reducing buckling capacity; as the magnitude of the imperfection increases, the influence of plastic deformation becomes less important. It is also found that the geometric parameter λ , which is used as an important factor in elastic response, becomes meaningless for the elastic-plastic buckling analysis of spherical caps.

INTRODUCTION

To realistically predict buckling loads for spherical caps, consideration should be given to the effect of geometric and material nonlinearities as well as initial imperfections, since all three factors play significant roles in reducing spherical cap buckling capacity.

The axisymmetric buckling of clamped shallow spherical shells were studied by Huang [1] and Weinitschke [2]. To reduce the gap between experiment and theory, they introduced asymmetrical deflections along the circumferential direction and obtained buckling pressures for different cap geometric parameters by solving eigenvalue problems.

Khojasteh-Bakht [3] analyzed small deflection elastic-plastic shells of revolution by the finite element method. Marcal extended the work of [3] to include large deformation terms [4]. An isotropic strain-hardening is assumed in these two references and it is found in Ref. [4] that the plastic yielding has the significant effect of reducing the buckling pressure of shell structures. Various solution procedures for the large deformation elastic-plastic analysis of shell structures were discussed in Ref. [5]. Shells of revolution under cyclic loading were examined in Ref. [6]. Bushnell [7] employed a variational finite-difference approach to investigate the influence of plastic deformation on a shell structure.

Initial imperfections in the shell shape sometimes accounted for the discrepancy between experimentally observed buckling loads and theoretically calculated values [8].

Hutchinson [9] utilized the Koiter approach to determine the approximate asymmetric buckling load of spherical shells with initial imperfections. Asymmetric buckling loads for spherical caps with asymmetric imperfections were obtained in Refs. [10,11] by directly solving two dimensional governing differential equations.

It is the purpose of this work to study the effect of initial imperfections, and geometrical and material nonlinearities on the axisymmetric buckling of spherical caps. It is hoped that the result obtained may provide a better understanding on the axisymmetric buckling nature of spherical caps. The analysis of the proposed title problem can be proceeded by incorporating the appropriate plasticity theory into an existing computer code [12].

Selection of a plasticity theory is very important. The theory should be simple in mathematical expression, easy to apply and capable of representing the material property such as the Bauschinger effect. In accordance with these criteria, the von Mises initial yield condition, the incremental flow theory [13] and the Prager-Ziegler kinematic hardening theory [14,15] are used in this study.

The problem formulation is based on equilibrium equations, treating the plastic deformation as effective plastic loads which are lumped together with actual applied loads [16]. Governing equations are replaced by finite differences and resulting equations are then solved by the nonlinear relaxation method [17].

In the next section, the governing equations based on

equilibrium considerations are given. This is followed by the description of plasticity relations and the general solution procedure. To test the validity of the plasticity theory adopted, example problems are solved and comparisons with other solutions are made. Large deformation elastic-plastic buckling loads are then obtained for spherical caps with initial imperfections. Conclusions and a general discussion are given in the final section.

PROBLEM FORMULATION

The geometry of a spherical cap is shown in Fig. 1a, in which H is the central height and R the shell radius; a is the base radius; $W(r)$ and $U(r)$ are the displacement components along normal and tangential directions, respectively, and $W_i(r)$ is the initial imperfection; q is the applied uniform pressure. The undeformed shape of the perfect shell can be adequately described by

$$z = H[1 - (r/a)^2] \quad (1a)$$

and the radius of curvature of the shell is approximated by

$$R = a^2/2H \quad (1b)$$

where r is the radial coordinate.

Fig. 1b shows the membrane forces N_r and N_θ , the transverse shear Q_r and the moments M_r and M_θ . Equilibrium of moments requires

$$(rM_r)' - M_\theta - rQ_r = 0 \quad (2)$$

And equilibrium of stress resultants along radial and normal directions provides

$$(rN_r)' - N_\theta = 0 \quad (3)$$

$$[rN_r(W_f - z)' + rQ_r]' + rq = 0 \quad (4)$$

where $()' = \partial() / \partial r$ and $W_f = W + W_i$. Note that the nonlinearity has been introduced in Eq. (4) by considering the influence of W_f .

Elimination of Q_r in Eqs. (2) and (4) yields

$$M_r'' + \frac{2}{r} M_r' - \frac{1}{r} M_\theta' + N_r(W_f'' + \frac{1}{R}) + N_\theta(\frac{W_f'}{R} + \frac{1}{R}) + q = 0 \quad (5)$$

Eqs. (3) and (5) are the basic equations for the analysis of axisymmetric spherical caps.

Stress-Strain and Strain-Displacement Relations

For a shell deforming into plastic range, the strain in a point within the thickness can be expressed by

$$\{e\} = \{e^e\} + \{e^p\} \quad (6)$$

where $\{e\}$, $\{e^e\}$ and $\{e^p\}$ are the total, elastic and plastic strain vectors, respectively.

Furthermore, the total strain can be considered as the sum of the membrane and bending components:

$$\{e\} = \{\epsilon\} + z\{\kappa\} \quad (7)$$

where z is the vertical coordinate through the shell thickness (Fig. 1b). The membrane and bending strains are related to displacements by

$$\begin{aligned} \epsilon_r &= U' - \frac{W}{R} + \frac{1}{2}(W')^2 + W'W'_i \\ \epsilon_\theta &= \frac{U}{r} - \frac{W}{R} \\ \kappa_r &= -W'' \\ \kappa_\theta &= -\frac{W'}{r} \end{aligned} \quad (8)$$

Note that the elastic components of strains are the only strains which can be related to stresses by Hook's law:

$$\{\sigma\} = [E](\{e\} - \{e^p\}) \quad (9)$$

where $[E]$, the elastic strain to stress transformation matrix, is given as

$$[E] = \frac{E}{1-\nu^2} \begin{bmatrix} 1 & \nu \\ \nu & 1 \end{bmatrix} \quad (10)$$

in which E is Young's modulus and ν is Poisson's ratio.

Membrane stress resultants and bending moments are obtained by

$$\{N\} = \int_{-h/2}^{h/2} \{\sigma\} dz \quad (11)$$

$$\{M\} = \int_{-h/2}^{h/2} \{\sigma\} z dz \quad (12)$$

Substituting Eqs. (6-9) into Eqs. (11) and (12), we obtain the membrane forces

$$\begin{Bmatrix} N_r \\ N_\theta \end{Bmatrix} = \frac{Eh}{1-\nu^2} \begin{bmatrix} 1 & \nu \\ \nu & 1 \end{bmatrix} \begin{Bmatrix} \epsilon_r \\ \epsilon_\theta \end{Bmatrix} - \begin{Bmatrix} N_r^P \\ N_\theta^P \end{Bmatrix} \quad (13)$$

where the effective plastic membrane forces are

$$\begin{Bmatrix} N_r^P \\ N_\theta^P \end{Bmatrix} = [E] \int_{-h/2}^{h/2} \begin{Bmatrix} e_r^P \\ e_\theta^P \end{Bmatrix} dz \quad (14)$$

and the moments

$$\begin{Bmatrix} M_r \\ M_\theta \end{Bmatrix} = D \begin{bmatrix} 1 & \nu \\ \nu & 1 \end{bmatrix} \begin{Bmatrix} \kappa_r \\ \kappa_\theta \end{Bmatrix} - \begin{Bmatrix} M_r^P \\ M_\theta^P \end{Bmatrix} \quad (15)$$

where $D = Eh^3/12(1-\nu^2)$, and effective plastic moments are

$$\begin{Bmatrix} M_r^P \\ M_\theta^P \end{Bmatrix} = [E] \int_{-h/2}^{h/2} \begin{Bmatrix} e_r^P \\ e_\theta^P \end{Bmatrix} z dz \quad (16)$$

Governing Equations

In terms of displacements, the governing equation involving the major displacement U is obtained by substituting Eqs. (13) and (14) into Eq. (3):

$$U'' + \frac{U'}{r} - \frac{U}{r^2} + G(W) = \frac{1-\nu^2}{Eh} q_1^p \quad (17)$$

where

$$G(W) = F'_r(W) + \nu F'_\theta(W) + \frac{1-\nu}{r}(F_r - F_\theta)$$

$$F_r(W) = -W/R + (W')^2/2 + W'W'_i$$

$$F_\theta(W) = -W/R \quad (18)$$

$$F'_r(W) = -W'/R + W'W'' + W'W''_i + W''W'_i$$

$$F'_\theta(W) = -W'/R$$

and q_1^P , an effective plastic load, is expressed in terms of effective plastic membrane forces by

$$q_1^P = (N_r^P)' + N_r^P/r - N_\theta^P/r \quad (19)$$

The governing equation involving the major displacement W is also obtained by substituting Eqs. (13-16) into Eq. (5):

$$\begin{aligned} DV^4 W - \frac{Eh}{1-\nu} \frac{1}{2} (\epsilon_r + \nu \epsilon_\theta) (W''_f + 1/R) - \frac{Eh}{1-\nu} \frac{1}{2} (\epsilon_\theta + \nu \epsilon_r) (W'_f/r + 1/R) \\ = q - q_2^P - q_3^P \end{aligned} \quad (20)$$

where $V^4 = \nabla^2(\nabla^2)$ and $\nabla^2(\) = (\)'' + (\)'/r$; the membrane strains $\epsilon_r, \epsilon_\theta$ are defined in Eqs. (8), effective plastic loads q_2^P and q_3^P are given as

$$q_2^P = N_r^P(W''_f + 1/R) + N_\theta^P(W'_f/r + 1/R) \quad (21)$$

$$q_3^P = (M_r^P)'' + 2(M_r^P)'/r - (M_\theta^P)'/r \quad (22)$$

Eqs. (17) and (20) are two fundamental governing equations in terms of displacements for the present analysis.

Boundary Conditions

At shell apex, the nature of axi-symmetry requires that

$$W'(0) = 0 \quad (23)$$

$$U(0) = 0 \quad (24)$$

Along the outer edge ($r=a$), if the cap is clamped:

$$U(a) = W(a) = W'(a) = 0 \quad (25)$$

On the other hand, if the cap is simply supported, it requires that

$$U(a) = W(a) = 0 \quad (26a)$$

and that $M_r(a)$ in Eq. (15) to be zero, i.e.

$$D\left(\frac{d^2W}{dr^2} + \frac{\nu}{r} \frac{dW}{dr}\right) = -M_r^p(a), \quad r=a \quad (26b)$$

where M_r^p is defined in Eq. (16).

Nondimensional Forms

For convenience, the following nondimensional quantities are introduced

$$\begin{aligned} x &= r/a & m^4 &= 12(1-\nu^2) \\ \lambda^2 &= m^2 a^2 / Rh & q_{cr} &= 4Eh^2 / R^2 m^2 \\ ()' &= \partial() / \partial x & p &= q / q_{cr} \\ u &= aU/h^2 & w_i &= W_i / h \\ w &= W/h \end{aligned} \quad (27)$$

where q_{cr} is the classical buckling pressure of a complete spherical shell of the same radius of curvature and thickness. With the adoption of Eqs. (27), the nondimensional forms of Eqs. (17) and (20) become

$$u'' + \frac{u'}{x} - \frac{u}{x^2} + g(w) = \frac{(1-\nu^2)a^3}{Eh^3} q_1^p \quad (28)$$

and

$$\begin{aligned}
 v^4 w - 12(\bar{\epsilon}_r + v\bar{\epsilon}_0) \left(w'' + \frac{\lambda^2}{m^2} \right) - 12(\bar{\epsilon}_\theta + v\bar{\epsilon}_r) \left(\frac{w'}{x} + \frac{\lambda^2}{m^2} \right) \\
 = 4 \frac{\lambda^4}{m^2} p - \frac{m^4 a^4}{Eh^4} (q_2^p + q_3^p)
 \end{aligned} \tag{29}$$

where $g(w)$ and $f(w)$ terms are nondimensional counterparts of similar terms in Eq. (18):

$$g(w) = f'_r(w) + v f'_\theta(w) + (1-v) [f_r(w) - f_\theta(w)] / x$$

$$f_r(w) = - \frac{\lambda^2}{m^2} w + \frac{1}{2} (w')^2 + w' w'_i$$

$$f_\theta(w) = - \frac{\lambda^2}{m^2} w \tag{30}$$

$$f'_r(w) = - \frac{\lambda^2}{m^2} w' + w' w'' + w' w''_i + w'' w'_i$$

$$f'_\theta(w) = - \frac{\lambda^2}{m^2} w'$$

and $\bar{\epsilon}_r, \bar{\epsilon}_\theta$ are nondimensional quantities of membrane strains ϵ_r and ϵ_θ in Eq. (8)

$$\bar{\epsilon}_r = u' - \frac{\lambda^2}{m^2} w + \frac{1}{2} (w')^2 + w' w''_i$$

$$\bar{\epsilon}_\theta = \frac{u}{x} - \frac{\lambda^2}{m^2} w$$

(31)

PLASTICITY RELATIONS

As indicated by Ziegler [15], the behavior of a strain-hardening material can be described by

- (a) an initial yield condition, defining the elastic limit of the material,
- (b) a flow rule, relating the plastic strain increment with the stress and the stress increment,
- (c) a hardening rule, specifying the subsequent yield condition in the course of plastic flow.

Because of complexity associated with plastic deformation, the laws governing the behavior of materials in the plastic range have not, as yet, reached a level of general acceptance. A judicious choice, among all available plasticity theories, should consider both the simplicity in mathematical expression and the proper representation of experimentally observed material behavior.

Based on these considerations, the von Mises yield function, which describes a smooth surface in stress space and represents a simple mathematical function, is chosen as the initial yield condition. The flow rule of von Mises and the Ziegler-Prager kinematic hardening rule are also selected in this study. It is important to note that this hardening rule does account for the Bauschinger effect.

In a 9-space stress field with origin 0 (Fig. 2), the von Mises initial yield surface can be described by

$$F(\sigma_{ij}) = k^2 = \text{constant} \quad (32)$$

For an initially isotropic material, the form of the function

F is invariant with respect to a rotation of the stress state.

The Prager's hardening rule [14] assumes that during plastic deformation, the yield surface moves in a translation without changing its shape and hence the subsequent yield surface takes the form

$$F(\sigma_{ij} - \alpha_{ij}) = k^2 \quad (33)$$

where α_{ij} represents the total translation of the yield surface center which is a measure of the degree of work hardening. In the space σ_{ij} , α_{ij} is the position vector of the yield surface center C which before plastic deformation takes place is located at the origin (Fig. 2).

The flow rule of von Mises gives the following expression:

$$de_{ij}^p = \frac{\partial F}{\partial \sigma_{ij}} d\lambda, \quad d\lambda > 0 \quad (34)$$

which indicates that the plastic strain increment de_{ij}^p lies in the exterior normal of the yield surface (33).

The Ziegler's modification [15] of Prager's hardening rule suggests that the surface (33) moves in the direction of the radius connecting its center with the stress point (Fig. 2):

$$d\alpha_{ij} = (\sigma_{ij} - \alpha_{ij}) d\mu, \quad d\mu > 0 \quad (35)$$

$d\lambda$ in Eq. (34) and $d\mu$ in Eq. (35) are to be determined.

Determination of $d\mu$ is based on the condition that stress point always remains on the yield surface in plastic flow. This condition, in fact, states that for an infinitesimal increment of loading the vector $d\sigma_{ij} - d\alpha_{ij}$ must be orthogonal to the outer normal to the yield surface:

$$(d\sigma_{ij} - d\alpha_{ij}) \frac{\partial F(\sigma_{ij} - \alpha_{ij})}{\partial \sigma_{ij}} = 0 \quad (36)$$

Substituting (35) into (36) yields

$$d\mu = \frac{(\partial F/\partial \sigma_{kl}) d\sigma_{kl}}{(\sigma_{mn}^{-\alpha_{mn}}) \partial F/\partial \sigma_{mn}} \quad (37a)$$

and hence

$$d\alpha_{ij} = \frac{(\partial F/\partial \sigma_{kl}) d\sigma_{kl}}{(\sigma_{mn}^{-\alpha_{mn}}) \partial F/\partial \sigma_{mn}} (\sigma_{ij}^{-\alpha_{ij}}) \quad (37b)$$

According to Refs. [14,15], $\partial \lambda$ in (34) can be obtained by assuming $d\alpha_{ij} = c d\epsilon_{ij}^p$ and putting this relation into (36):

$$d\lambda = \frac{1}{c} \frac{(\partial F/\partial \sigma_{kl}) d\sigma_{kl}}{(\partial F/\partial \sigma_{mn}) (\partial F/\partial \sigma_{mn})} \quad (38a)$$

and hence

$$d\epsilon_{ij}^p = \frac{1}{c} \frac{(\partial F/\partial \sigma_{kl}) d\sigma_{kl}}{(\partial F/\partial \sigma_{mn}) (\partial F/\partial \sigma_{mn})} \frac{\partial F}{\partial \sigma_{ij}} \quad (38b)$$

where c is the hardening coefficient and can be determined from the uniaxial stress-strain relation.

Now, let us write Eq. (33) in terms of 3 principal stresses:

$$\begin{aligned} f &= F - k^2 \\ &= \frac{1}{2} [(\bar{\sigma}_1 - \bar{\sigma}_2)^2 + (\bar{\sigma}_2 - \bar{\sigma}_3)^2 + (\bar{\sigma}_3 - \bar{\sigma}_1)^2] - \sigma_y^2 = 0 \end{aligned} \quad (39)$$

where σ_y is the yield stress in uniaxial tension and $\bar{\sigma}_1 = \sigma_1^{-\alpha_1}$, $\bar{\sigma}_2 = \sigma_2^{-\alpha_2}$, $\bar{\sigma}_3 = \sigma_3^{-\alpha_3}$.

For the case of plane stress (Fig. 3), we have

$$\sigma_3 = \alpha_3 = \bar{\sigma}_3 = 0 \quad (40)$$

and Eq. (39) reduces to

$$f = \bar{\sigma}_1^2 - \bar{\sigma}_1 \bar{\sigma}_2 + \bar{\sigma}_2^2 - \sigma_y^2 = 0 \quad (41)$$

By putting Eq. (39) into Eq. (38b) and using relations (40-41),

we obtain

$$\begin{Bmatrix} \Delta e_1^p \\ \Delta e_2^p \end{Bmatrix} = \frac{1}{D} \begin{bmatrix} S_1^2 & S_1 S_2 \\ S_1 S_2 & S_2^2 \end{bmatrix} \begin{Bmatrix} \Delta \sigma_1 \\ \Delta \sigma_2 \end{Bmatrix} \quad (42)$$

where

$$S_1 = (\bar{\sigma}_1 - \bar{\sigma}_2)/2 / \sigma_y, \quad S_2 = (\bar{\sigma}_2 - \bar{\sigma}_1)/2 / \sigma_y, \quad D = \frac{3}{2} c \quad (43)$$

From Hook's law, we have

$$\begin{Bmatrix} \Delta \sigma_1 \\ \Delta \sigma_2 \end{Bmatrix} = \frac{E}{1-\nu^2} \begin{bmatrix} 1 & \nu \\ \nu & 1 \end{bmatrix} \begin{Bmatrix} \Delta e_1^e \\ \Delta e_2^e \end{Bmatrix} \quad (44)$$

It is also noted that

$$\begin{Bmatrix} \Delta e_1^e \\ \Delta e_2^e \end{Bmatrix} = \begin{Bmatrix} \Delta e_1 \\ \Delta e_2 \end{Bmatrix} - \begin{Bmatrix} \Delta e_1^p \\ \Delta e_2^p \end{Bmatrix} \quad (45)$$

Introducing (42) into (44) provides

$$\begin{Bmatrix} \Delta \sigma_1 \\ \Delta \sigma_2 \end{Bmatrix} = \begin{bmatrix} C_{11} & C_{12} \\ C_{21} & C_{22} \end{bmatrix} \begin{Bmatrix} \Delta e_1 \\ \Delta e_2 \end{Bmatrix} \quad (46)$$

where

$$C_{11} = \frac{E}{\Omega} (D + E S_2^2)$$

$$C_{12} = \frac{E}{\Omega} (D\nu - E S_1 S_2) = C_{21}$$

$$C_{22} = \frac{E}{\Omega} (D + E S_1^2)$$

$$\Omega = D(1-\nu^2) + E(S_1^2 + 2\nu S_1 S_2 + S_2^2)$$

For a given displacement field, $\{\Delta e\}$ are obtained from incremental forms of Eqs. (7) and (8). Eqs. (46) are the stress-strain relations during the course of plastic flow (loading). Otherwise, Eqs. (44) should be used for all stress computations.

Up to this point, the hardening coefficient c in Eq. (43) is the only constant yet to be decided. If the structure is in a state of uniaxial stress, the stress-strain relation is the same as that obtained from tension or compression tests. The expression for the hardening coefficient c can be readily obtained from Eq. (42) by setting $\Delta e^P = \Delta e_1^P$, $\Delta \sigma = \Delta \sigma_1$:

$$\frac{1}{c} = \frac{3}{2} \frac{\Delta e^P}{\Delta \sigma} \quad (47a)$$

or

$$D = \frac{\Delta \sigma}{\Delta e^P} \quad (47b)$$

This equation shows that the value of D is equal to the slope of the uniaxial stress-plastic strain curve.

From Eqs. (47), the values of the hardening coefficient for two special cases may be specified here: (i) for an elastic-ideally plastic material, $c=D=0$, (ii) for a linear hardening material, $D=EE_t/(E-E_t)$, where E_t is the tangent modulus. Uniaxial stress-strain curves for these two types of hardening material are given in Fig. 4.

Nonlinear Hardening

Also given in Fig. 4 is the stress-strain curve for a nonlinear hardening material. Its D value, instead of being a constant, depends on the state of stress. One way of dealing with this rather complicate situation is based on the Ramberg-Osgood representation of a uniaxial stress-strain curve [18]:

$$e = \frac{\sigma}{E} + \frac{3\sigma}{7E} \left| \frac{\sigma}{\sigma_{0.7}} \right|^{n-1} \quad (48)$$

$$\text{where } n = 1 + \frac{\log(17/7)}{\log(\sigma_{0.7}/\sigma_{0.85})}$$

e is the total strain, E is the slope of the linear portion of the stress-strain curve, and $\sigma_{0.7}$ and $\sigma_{0.85}$ are the stresses at which the curve has secant moduli of $0.7E$ and $0.85E$, respectively.

It is understood that the nonlinear term in Eq. (48) is the plastic strain. D value of this material can be obtained as

$$D = \frac{7E}{3n} \left| \frac{\sigma_{0.7}}{\sigma} \right|^{n-1} \quad (49a)$$

We may generalize this equation to a multiaxial state of stress [19,20]:

$$D = \frac{7E}{3n} \left| \frac{\sigma_{0.7}}{\bar{\sigma}} \right|^{n-1} \quad (49b)$$

where $\bar{\sigma}$, the effective stress, is defined as

$$\bar{\sigma} = \sqrt{\frac{3}{2} \sigma'_{ij} \sigma'_{ij}} \quad (50a)$$

in which σ'_{ij} is the deviatoric stress. For the case of plane stress,

$$\bar{\sigma} = \sigma_1^2 - \sigma_1 \sigma_2 + \sigma_2^2 \quad (50b)$$

Loading Criteria

In the incremental solution procedure for elastic-plastic problems, in addition to the constitutive relations, it is necessary to have a loading/unloading criterion. For this purpose, let's define $\dot{f} = (\partial f / \partial \sigma_{ij}) d \sigma_{ij}$, where f has been defined in Eq. (39). Loading, unloading and neutral loading are associated with the plastic state $f=0$, and are

characterized by $\dot{f} > 0$, $\dot{f} < 0$ and $\dot{f} = 0$, respectively. When loading or neutral loading takes place, Eq. (46) must be applied. On the other hand, Eq. (44) must be used when unloading occurs.

SOLUTION PROCEDURE

For convenience, a simple flow chart is sketched in Fig. 5 to explain the general solution procedure. The entire process is divided into two major loops, namely, the elastic solution and material property loops.

In the elastic solution loop, all material properties are held constant. Consequently, the effective plastic loads, q_i^p in the two governing equations (28) and (29) are fixed and combined with the actual externally applied load q , the problem is thus reduced to an elastic large deformation problem.

Central finite differences are used to convert Eqs. (28) and (29) to a discrete system of equations, and the nonlinear relaxation technique is employed to solve these nonlinear equations. For details of solving these equations by the nonlinear relaxation technique, readers are referred to Ref. [17]. The iteration in this loop is considered converged when the average absolute change of u and w displacements at all points is less than 0.0001.

With the new displacement field $\{u\}^k$, the material properties must be updated so that the (nonlinear) stress-strain relation can be satisfied at all points over the shell surface and through the thickness. In the material property loop, the loading criterion is first checked. If the material point is in an unloading situation or still in the elastic range, Hook's law is used and the computation is very straight-forward.

If the material point is in a loading situation, incremental strains $\{\Delta e\}$ are computed from Eq. (7) by using

$\{\Delta u\} = \{u\}^k - \{u\}^{k-1}$ (where k is the number of the material property loop, see Fig. 5), and $\{\Delta \sigma\}$ are computed from Eq. (46). Having obtained $\{\Delta \sigma\}$, the new values of $\{\sigma\}$, $\{e^e\}$ and $\{e^p\}$ can readily be calculated. Effective plastic loads q_1^p are then evaluated from integration formulae (19), (21) and (22) through the use of Simpson's rule (9 thickness points are used for the entire computation in this paper).

The material property is considered to be updated if average absolute change of displacements between the present and the previous material property loop is less than 0.001. Otherwise, the iteration goes to the elastic solution loop again and the entire operation is repeated until the material property and equilibrium equations are satisfied.

COMPARISON WITH EXISTING SOLUTIONS

To test the validity and accuracy of plasticity theory utilized in this study, three small deformation circular plates and two large displacement spherical caps of various material properties are chosen as example problems.

The first example is a uniformly-loaded simply supported circular plate (Fig. 6a). Elastic-ideally plastic material is assumed with the value of the fully plastic moment, M_0 , equal to 4000 lb in/in. 11 and 9 points are selected along the plate surface and thickness, respectively. After the elastic limit has reached the load was increased in increments of 4 to 5 psi.

Results are displayed in Fig. 6a-6c; also shown in these figures are solutions of Ref. [21]. Ref. [21] adopted a finite element formulation and the isotropic hardening rule. Despite differences in the method of solution, these two sets of results are virtually identical.

Also shown in these figures are solutions from the elastic analysis. A redistribution of displacements and moments as a result of the plastic deformation is quite apparent in these figures.

The same example problem is considered again with the exception that the material property is of linear hardening behavior as given in Fig. 7a and 7b. The same surface and thickness points are used and results are displayed in Fig. 7a and 7b. Also plotted in these figures are elastic solutions and those calculated by Khojasteh-Bakht [3]. He used a finite element analysis and an isotropic hardening rule. Comparison of present results

and those of [3] is excellent. Again, the effect of the plastic deformation on displacements and moments is obvious from these figures.

The third example problem is a uniformly loaded clamped circular plate of nonlinear hardening material (Fig. 8a). This problem was originally considered in Ref. [22]. The material stress-strain curve given in Ref. [22] can be described by the following Ramberg-Osgood parameters: $E = 10^7$ psi, $\sigma_{0.7} = 24 \times 10^3$ psi, $n = 6.66$, $\sigma_y = 16 \times 10^3$ psi and $\nu = 0.33$. Present solutions and those of Refs. [19,22] are shown in Figs. 8a and 8b. The finite element method and kinematic hardening rule are used in Ref. [19]. On the other hand, a finite element formulation together with an isotropic hardening rule are employed in Ref. [22]. Good agreement is observed between present solutions and those of [22]. At higher load levels, results of Ref. [19] drift away from present solutions and those of Ref. [22].

Next we consider a simply-supported isotropic spherical cap under a uniform external pressure. Svalbonas and Levine predicted an elastic-plastic buckling load for such a cap in Ref. [20]. The material under consideration obeys a linear hardening law with a ratio of tangent modulus to Young's modulus of 0.1 and yield stress to Young's modulus of 0.002. A shell geometry parameter $\lambda = 4$ is chosen. Other geometric quantities are given in Fig. 9. Also shown in this figure are the present load vs central deflection curve and that of [20]. Comparison between these two sets of solutions is quite good; the present analysis predicts a buckling load of 2050 psi

which is about 5% below the value of 2150 psi estimated in [20].

The final example problem considered is a uniformly loaded clamped spherical cap of linear hardening material (Fig. 10). Geometric dimensions and material properties are the same as those of Fig. 9 except the thickness. Two geometric parameters of $\lambda=4$ and 5.5 obtained by varying the shell thickness are analyzed. Load vs central deflection curves are plotted in Fig. 10. Also shown in this figure are the results obtained in Ref. [6]. Good agreement between these two solutions are noted for the spherical caps of both $\lambda=4$ and 5.5. The present analysis predicts buckling occurs at load of 2060 psi for $\lambda=4$ and 1060 psi for $\lambda=5.5$.

ELASTIC-PLASTIC BUCKLING OF SPHERICAL CAPS WITH INITIAL IMPERFECTIONS

Having established the validity of plasticity theory adopted in this work, we turn our attention to the main objective of this paper: the large deformation elastic-plastic buckling analysis of spherical caps with initial imperfections.

Two types of spherical caps (called shells A and B in Fig. 11) are chosen with considerable difference in geometrical dimensions. Shell A is the same as that shown in Fig. 10; shell B was used in Ref. [23] for the dynamic buckling analysis. Three geometric parameters, $\lambda=5, 7.5$ and 10 , for each type of the spherical caps are selected for this study, the value of λ is obtained by varying the shell thickness h ($\lambda = 2[3(1-\nu^2)]^{1/4} (H/h)^{1/2}$). Material properties of these two spherical caps are given in Fig. 11; in both cases, only linear hardening is considered.

The axisymmetric initial imperfection adopted in this study is of the dimple type which was also used in Ref. [8]. The type of imperfection is expressed mathematically as

$$w_i = (W_{i0}/h) (1-x^2)^3$$

where W_{i0} is the maximum imperfection which occurs at the shell apex. Selection of this expression is, in fact, quite arbitrary. However, it does provide an adequate description for actual shells since the important parameter is the maximum eccentricity and not the imperfection shape function.

In the buckling analysis of spherical caps with the non-linearity in both geometry and material, time consuming

iteration schemes are usually involved, and hence an efficient numerical procedure is highly desired. The computer program developed in this study provides a restarting capability at any load level. Thus, in the buckling load calculation, it is able to halt the execution at any load level and restart from that point by a proper choice of load increments. Also, it is able to restart from the last converged load level by selecting a smaller load step after the iteration fails because of load level already advancing into the buckling zone. With this facility, more accurate buckling loads may be obtained, and considerable computing time may also be saved.

A geometric parameter of $\lambda=5$ is first studied. This corresponds to $h=0.26$ in. and 0.0227 in. for shells A and B, respectively. The magnitude of imperfections considered are $W_{10}/h=0, 0.1, 0.5$ and 1 . Results associated with this geometric parameter are depicted in Fig. 11 for buckling load vs imperfection. They include the elastic solution and those from elastic-plastic (linear hardening) analyses. It is important to point out that both shells A and B yield the same elastic solution. However, their elastic-plastic results are different.

For the purpose of references, load vs central deflection curves are plotted in Fig. 12 for $\lambda=5$ of shell A for different imperfections. Both elastic, elastic-plastic solutions are shown. A redistribution of displacements as a result of the plastic deformation is obvious from this figure.

Similar to what is shown in Fig. 11, the results for $\lambda=7.5$ and 10 are given in Figs. 13 and 14, respectively. Again, both shells A and B provide the same elastic solution for each

of $\lambda=7.5$ and 10. It is also noted that both solutions from elastic and elastic-plastic analyses are the same for shell B in Fig. 14. This means that the shell with this geometric parameter has the thickness so thin that it never does allow plastic deformation to develop before buckling occurs. The effect of the thickness dimension on plastic yielding can also be seen from a comparison of results among Figs. 11, 13 and 14: the larger the thickness, the more the influence of the plastic deformation. A summary of results presented in Figs. 11, 13 and 14 is given in Table 1.

Table 1 Buckling loads for clamped axisymmetric spherical caps

$\frac{W_{i0}}{h}$	λ							
	5		7.5		10			
	Elastic shell A	Elastic-plastic shell B	Elastic shell A	Elastic-plastic shell B	Elastic shell A	Elastic-plastic shell B		
0	.64	.31	.50	.58	.89	.85	.83	.85
.1	.54	.28	.43	.58	.89	.82	.81	.82
.5	.32	.20	.27	.52	.84	.71	.71	.71
1.0	.15	.12	.15	.29	.31	.54	.54	.54

DISCUSSION AND CONCLUSIONS

An incremental flow theory based on von Mises yield surface and in conjunction with the Prager-Ziegler kinematic hardening rule is utilized for the calculation of plastic deformations. The theory is then incorporated into an existing program for the large deformation analysis of spherical caps with initial imperfections. The problem formulation is based on equilibrium equations in which the plastic deformation is treated as an effective plastic load and lumped together with the actual applied loads.

In every solution cycle, the material property and effective plastic loads are held constant, and the problem is reduced to an elastic one whose solutions are obtained by finite differences and the nonlinear relaxation technique [17]. Effective plastic loads are then modified and the procedure is repeated until they correspond to the computed state of stress and to specified stress-strain relations at all points over the shell surface and through the thickness. The solution procedure mentioned here is sketched in Fig. 5 for reference.

It is noted that the kinematic hardening rule utilized in this work accounts for the Bauschinger effect, and that perfectly plastic, linear and nonlinear hardening behavior are all included in the program. Nine thickness points and a Simpson rule are used for the calculation of the plastic deformation. A dimple type of imperfection is adopted which provides a quite adequate description of the local nature of spherical shells.

In general, the convergence related to material property iterations is quite rapid. For example, for a load level not too close to the buckling zone and with a proper load increment, only about 2-5 iterations are usually required to satisfy the material property.

To test the validity of the plasticity theory implemented in the existing program [12], five elastic-plastic plate and spherical cap problems were solved. Good agreement with other solutions was obtained.

Large deformation, elastic-plastic buckling loads are calculated for two types of spherical caps (Fig. 11). For each of these caps, three geometric parameters (λ) are studied. Results obtained for each of these three parameters are presented in Figs. 11, 13 and 14, respectively. From these results, it is found that both initial imperfection and plastic deformation have the same effect of reducing buckling capacity, and that as the magnitude of imperfection increases, the influence of the plastic deformation becomes less significant. For example, at $W_{i0}/h=1$, elastic and elastic-plastic solutions are almost the same in Figs. 11, 13 and 14. It is also found that the geometric parameter λ , which is used as an important factor in elastic buckling load calculations, becomes meaningless for the elastic-plastic buckling analysis of these caps. Elastic-plastic buckling loads, in fact, depend on actual cap geometric dimensions and material properties.

As a final remark, the plasticity theory adopted in this work, due to its simplicity in the mathematical representation, is quite easy to apply. More importantly, because of its capacity of predicting an ideal Bauschinger effect, the theory

also provides very realistic results. The later feature is essential for the analysis of cases involving reversed or cyclic loading situations.

ACKNOWLEDGMENT

The author is deeply indebted to Dr. N. Perrone, Office of Naval Research, for his helpful suggestions and discussions during the course of this investigation.

REFERENCES

1. Huang, N. C., "Unsymmetric Buckling of Thin Shallow Spherical Shell," Journal of Applied Mechanics, Vol. 31, No. 3, Sept. 1964, pp. 447-457.
2. Weinitschke, H. J., "On Asymmetric Buckling of Shallow Spherical Shells," Journal of Mathematical Physics, Vol. 44, 1965, p. 141.
3. Khojasteh-Bakht, M., "Analysis of Elastic-Plastic Shells of Revolution Under Axisymmetric Loading by the Finite Element Method," Ph.D. thesis, University of California, Berkeley, 1967.
4. Marcal, P. V., "Large Deflection Analysis of Elastic-Plastic Shells of Revolution," AIAA Journal, Vol. 8, No. 9, Sept. 1970.
5. Stricklin, J., Haisler, W., and Von Riesenmann, W., "Formulation, Computation, and Solution Procedures for Material and/or Geometric Nonlinear Structural Analysis by the Finite Element Method," Texas A&M University and Sandia Corporation Report SC-CR-72-3102, January 1972.
6. Levine, H. S., Armen, H., Jr., Winter, R., and Pifko, A., "Nonlinear Behavior of Shells of Revolution Under Cyclic Loading," Computers and Structures, Vol. 3, 1973, pp. 589-617.
7. Bushnell, D., "Large Deflection Elastic-plastic Creep Analysis of Axisymmetric Shells," Numerical Solution of Nonlinear Structural Problems, Proceedings of ASME Winter Meeting, Nov. 1973.
8. Koga, T., and Hoff, N. J., "The Axisymmetric Buckling of Initially Imperfect Complete Spherical Shells," International Journal of Solids and Structures, July 1969.
9. Hutchinson, J. W., "Imperfection Sensitivity of Externally Pressurized Spherical Shells," Journal of Applied Mechanics, Vol. 34, No. 1, March 1967, pp. 49-55.
10. Kao, R., and Perrone, N., "Asymmetric Buckling of Spherical Caps with Asymmetric Imperfections," Journal of Applied Mechanics, Vol. 38, No. 1, March 1971.
11. Kao, R., "A Note on Buckling of Spherical Caps with Initial Imperfection," Journal of Applied Mechanics, Vol. 39, No. 3, Sept. 1972.
12. Kao, R., and Perrone, N., "Dynamic Buckling of Axisymmetric Spherical Caps with Initial Imperfections," Computers and Structures, Vol. 9, 1978, pp. 463-473.
13. Hill, R., The Mathematical Theory of Plasticity, Oxford

Univ. Press, 1950.

14. Prager, W., "The Theory of Plasticity: A Survey of Recent Achievements," (James Clayton Lecture), Proc. Instn. Mech. Engrs., Vol. 169, 1955, p. 41.
15. Ziegler, H., "A Modification of Prager's Hardening Rule," Quart. Appl. Math., Vol. 17, No. 1, 1959.
16. Lin, T. H., Theory of Inelastic Structures, John Wiley and Son, New York, 1968.
17. Perrone, N., and Kao, R., "A General Nonlinear Relaxation Technique for Solving Nonlinear Problems in Mechanics," J. of Applied Mechanics, Vol. 38, No. 2, June 1971, pp. 371-376.
18. Ramberg, W., and Osgood, W. R., "Description of Stress-Strain Curves by Three Parameters," NACA TN 902, 1943.
19. Armen, H., Jr., Pifko, A., and Levin, H. S., "Finite Element Analysis of Structures in the Plastic Range," NASA CR-1649, February 1971.
20. Svalbonas, V., and Levine, H., "Numerical Nonlinear Inelastic Analysis of Stiffened Shells of Revolution," Vol. I - Theory Manual for STARS-2P Digital Computer Program, NASA CR-2559, July 1975.
21. Popov, E. P., Khojesteh-Bakht, M., and Yaghmai, S., "Analysis of Elastic-Plastic Circular Plates," J. of Eng. Mechanics Div., ASCE, Vol. 93, No. EM6, December 1967, pp. 49-65.
22. Popov, E. P., Khjojasteh-Bakht, M., and Yaghmai, S., "Bending of Circular Plates of Hardening Material," Int. J. Solids and Structures, Vol. 3, 1967, pp. 975-988.
23. Stricklin, J. A., et al., "Nonlinear Dynamic Analysis of Shells of Revolution by Matrix Displacement Method," AIAA Journal, Vol. 9, No. 4, April 1971, pp. 629-636.

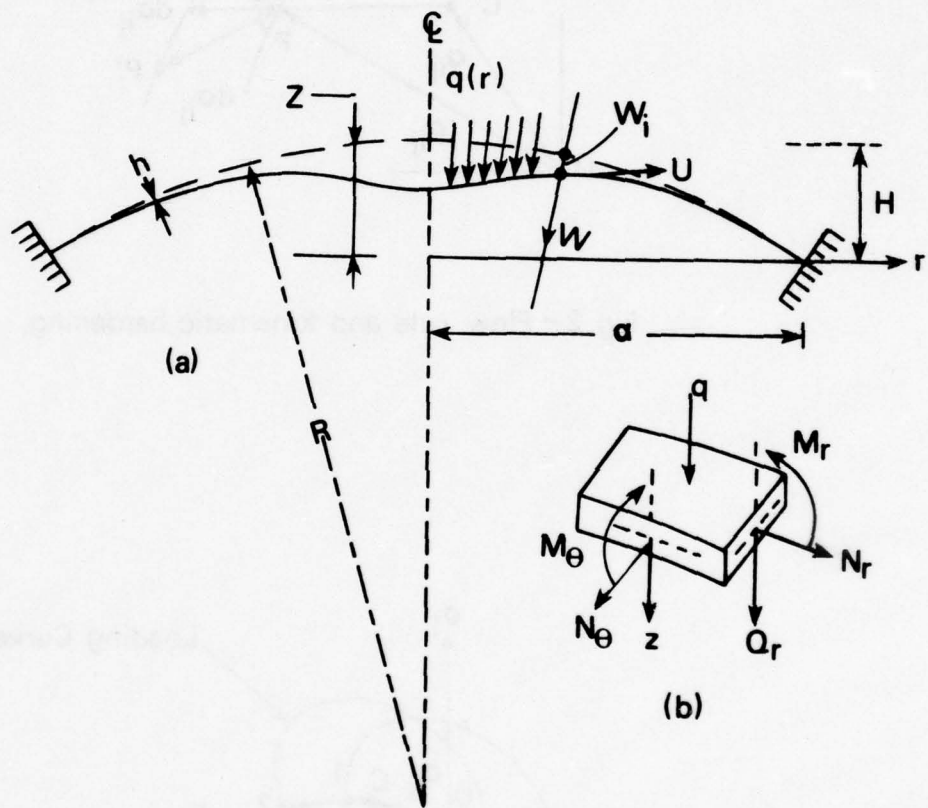


Fig.1 - Geometry, stress resultants and moments for axisymmetric clamped spherical cap with initial imperfection.

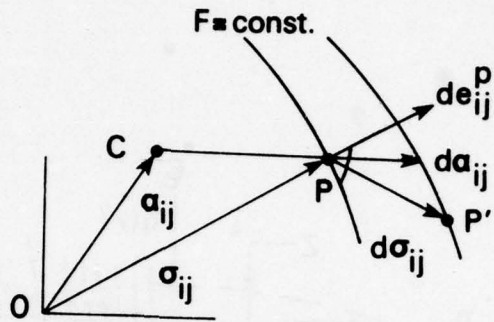


Fig. 2 - Flow rule and kinematic hardening.

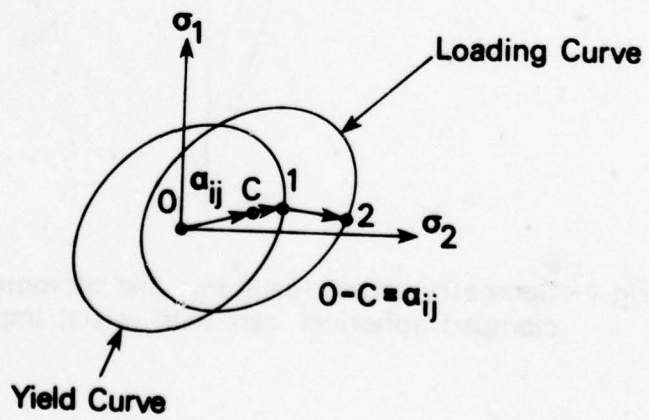


Fig. 3 - Kinematic hardening in plane stress.

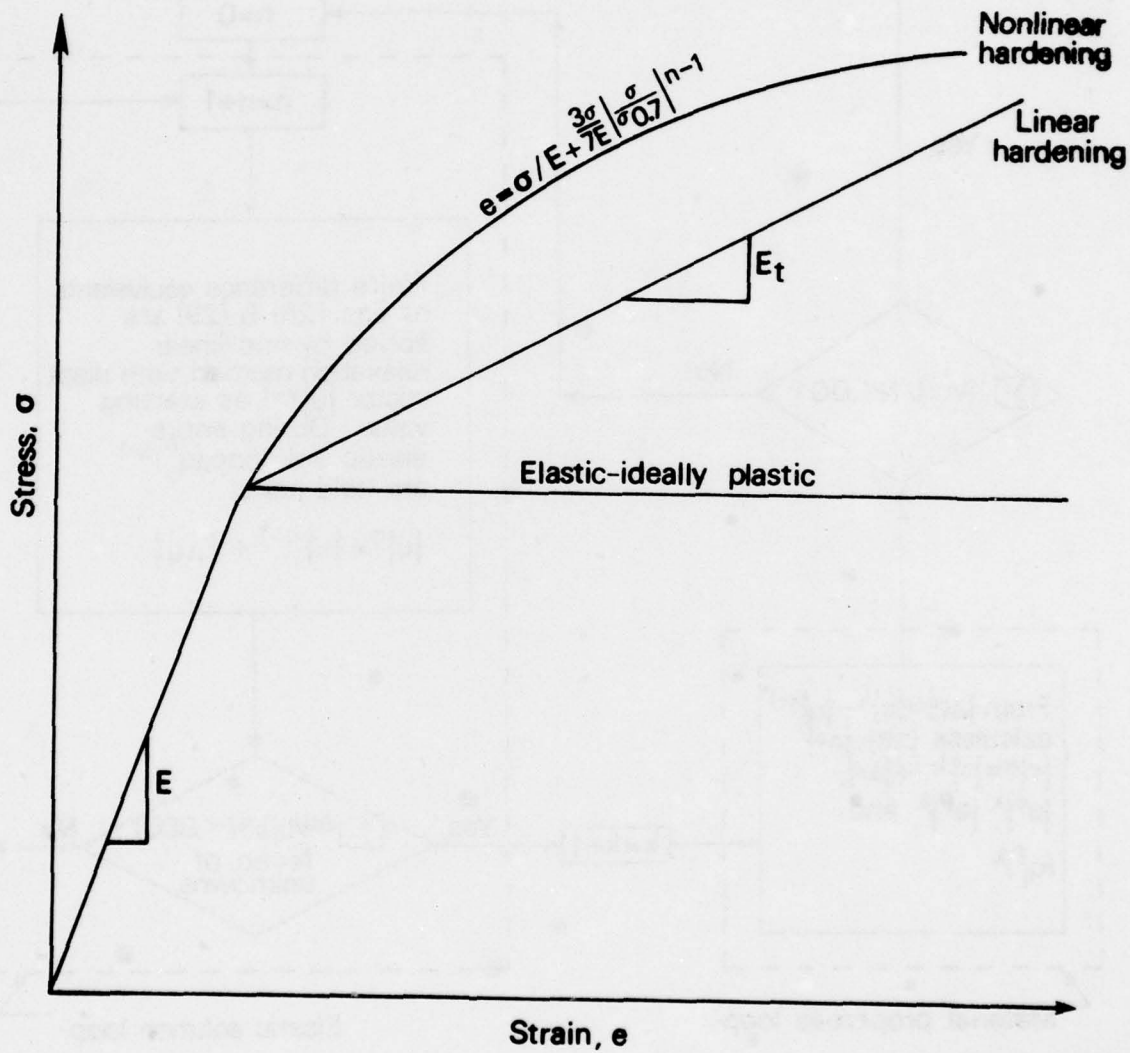


Fig. 4 - Nonlinear stress-strain curves
(three types of hardening).

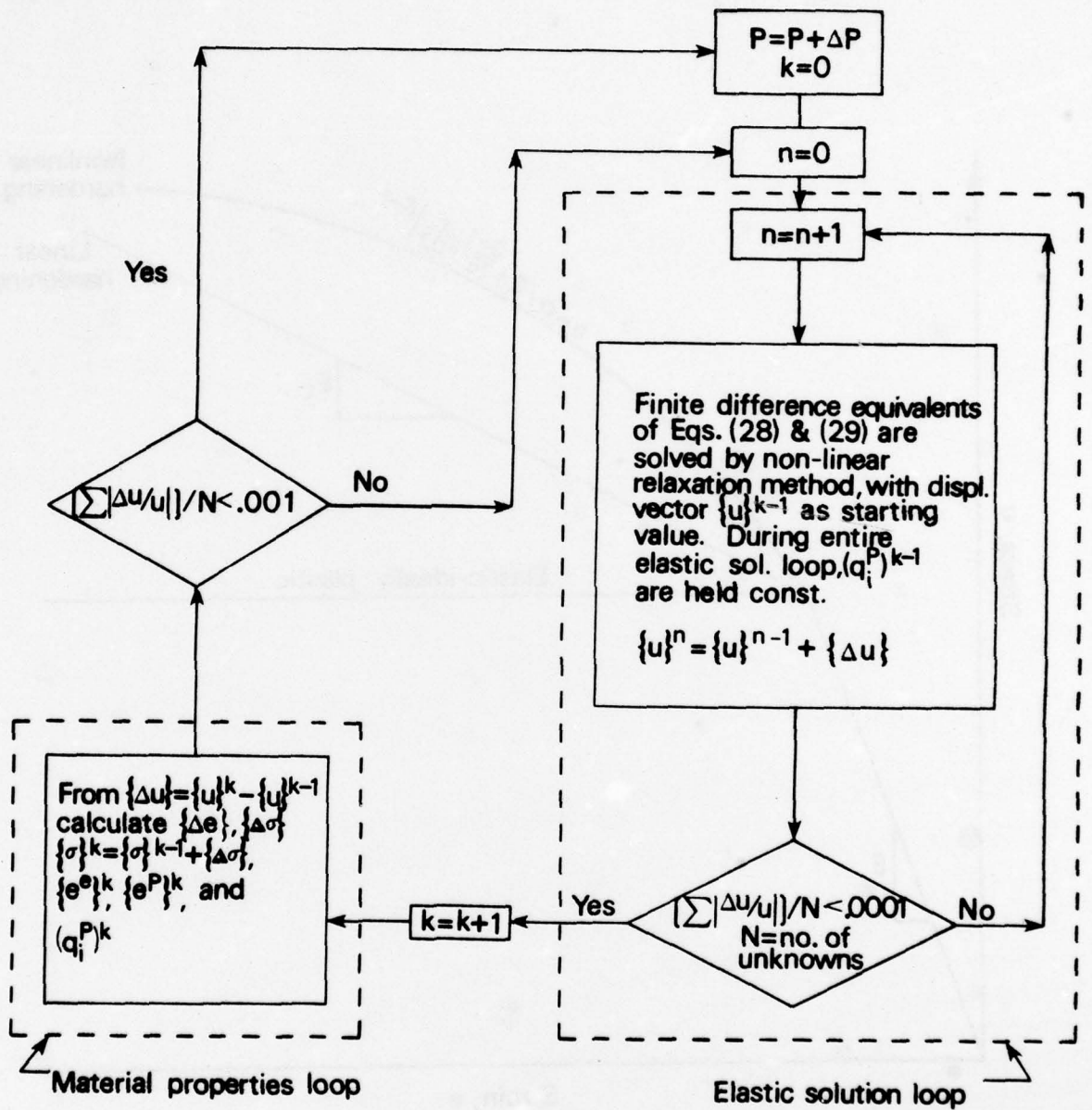


Fig. 5 - Iteration procedure for large deformation elastic-plastic problems.

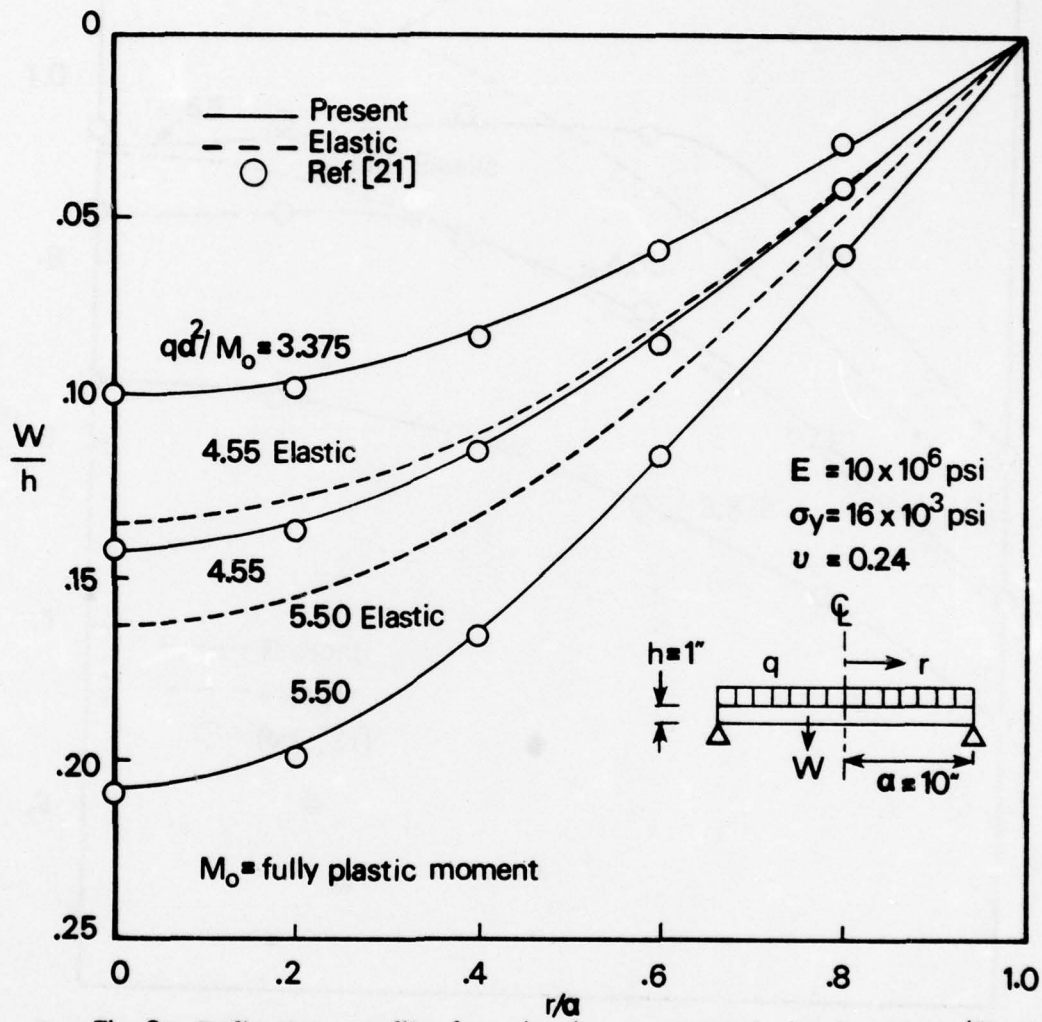


Fig. 6a-Deflection profile for simply supported circular plate (Elastic-ideally plastic).

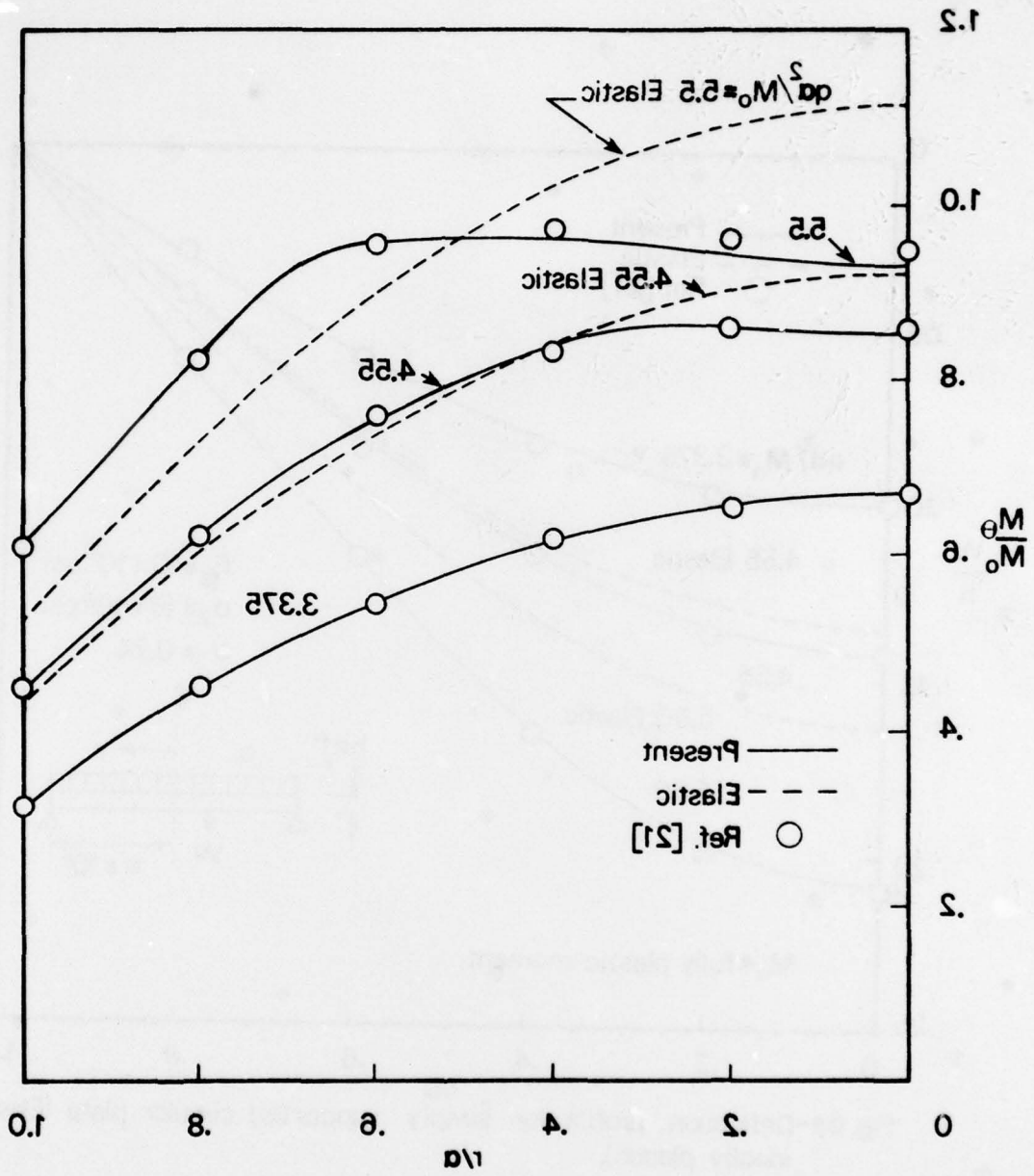


Fig 6b - Distribution of circumferential moment for simply supported circular plate (Elastic-ideally plastic).

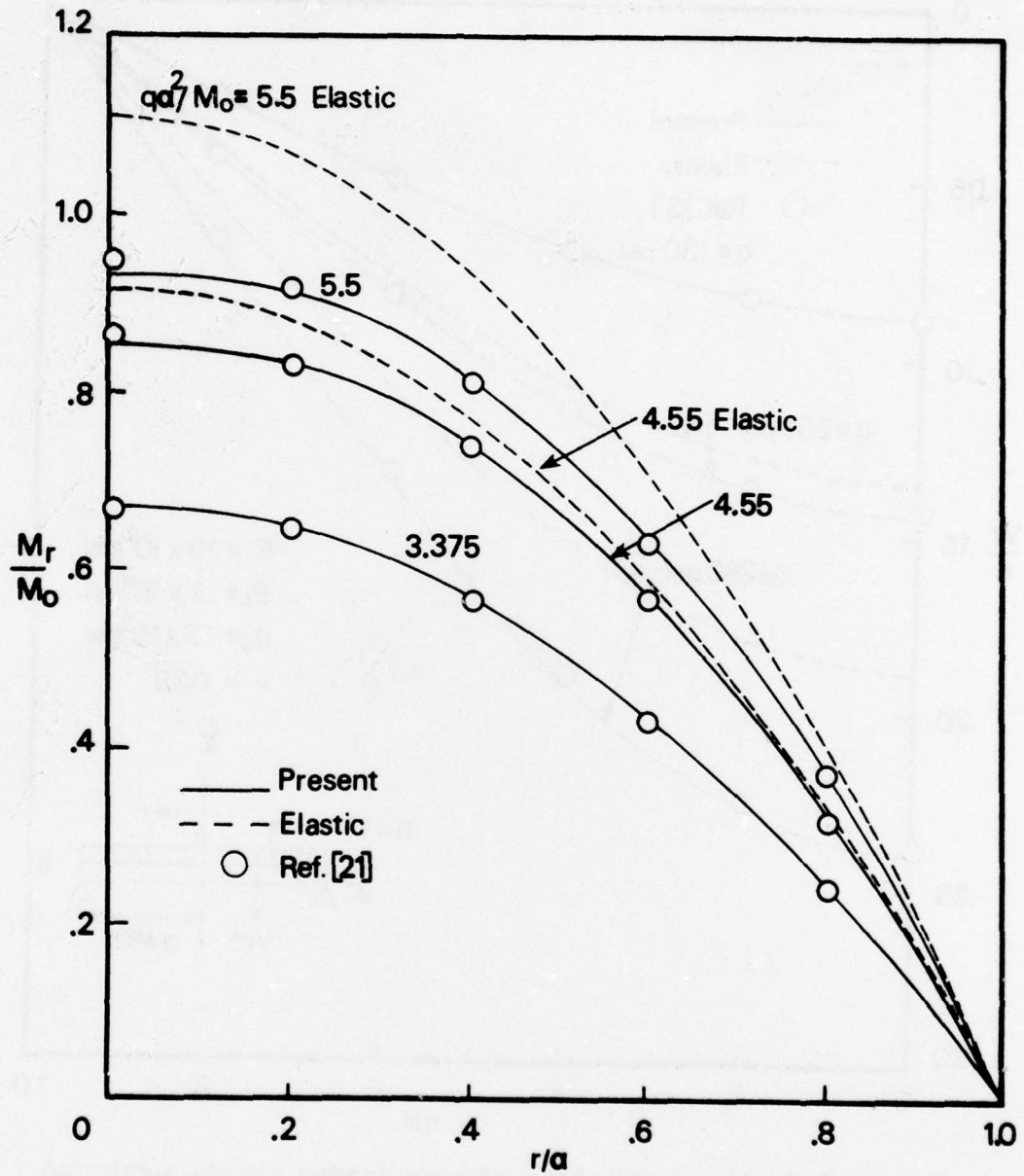


Fig. 6c - Distribution of radial moment for simply supported circular plate (Elastic-ideally plastic).

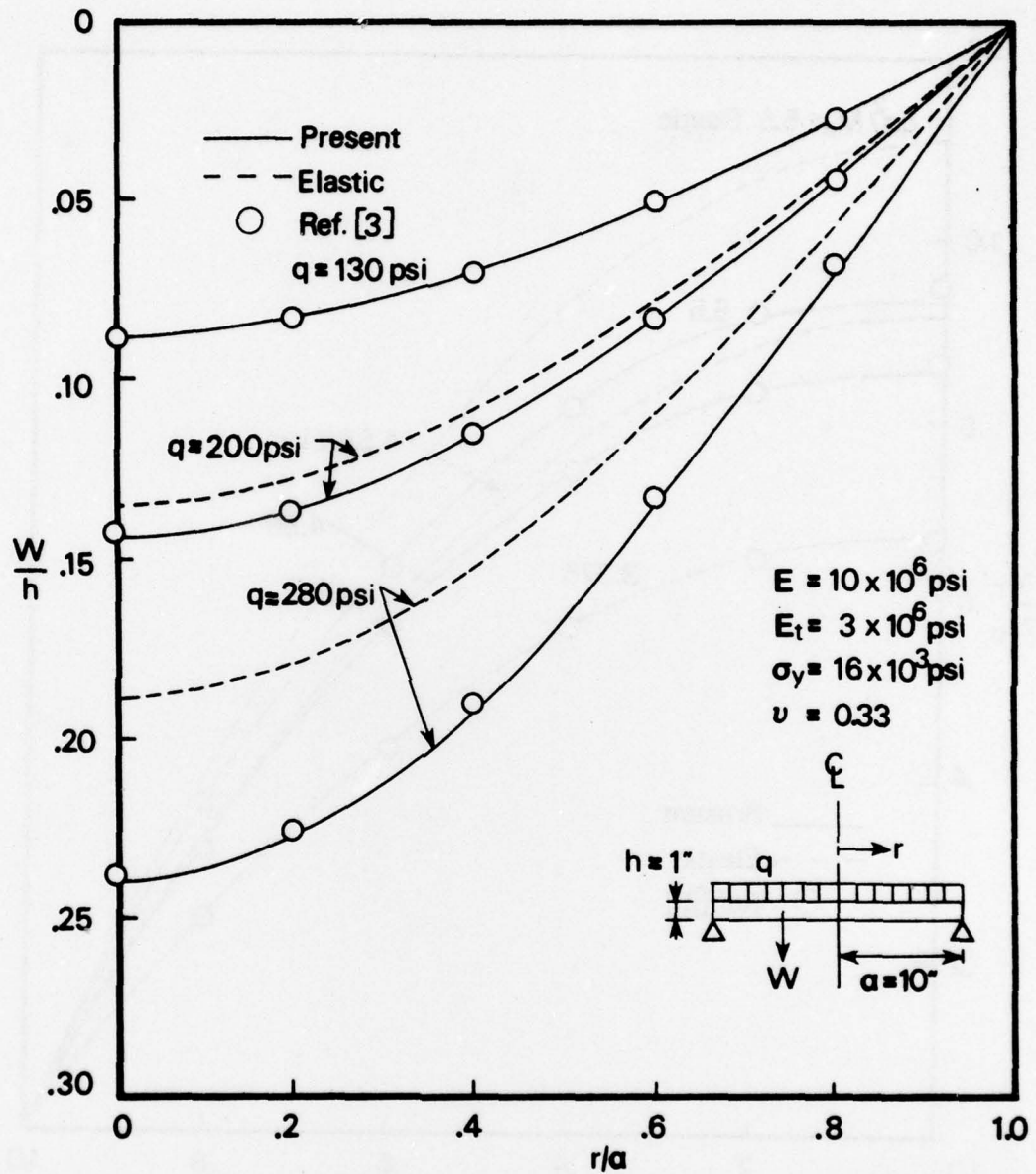


Fig. 7a-Deflection profile for uniformly loaded simply supported circular plate (Elastic-linear strain hardening).

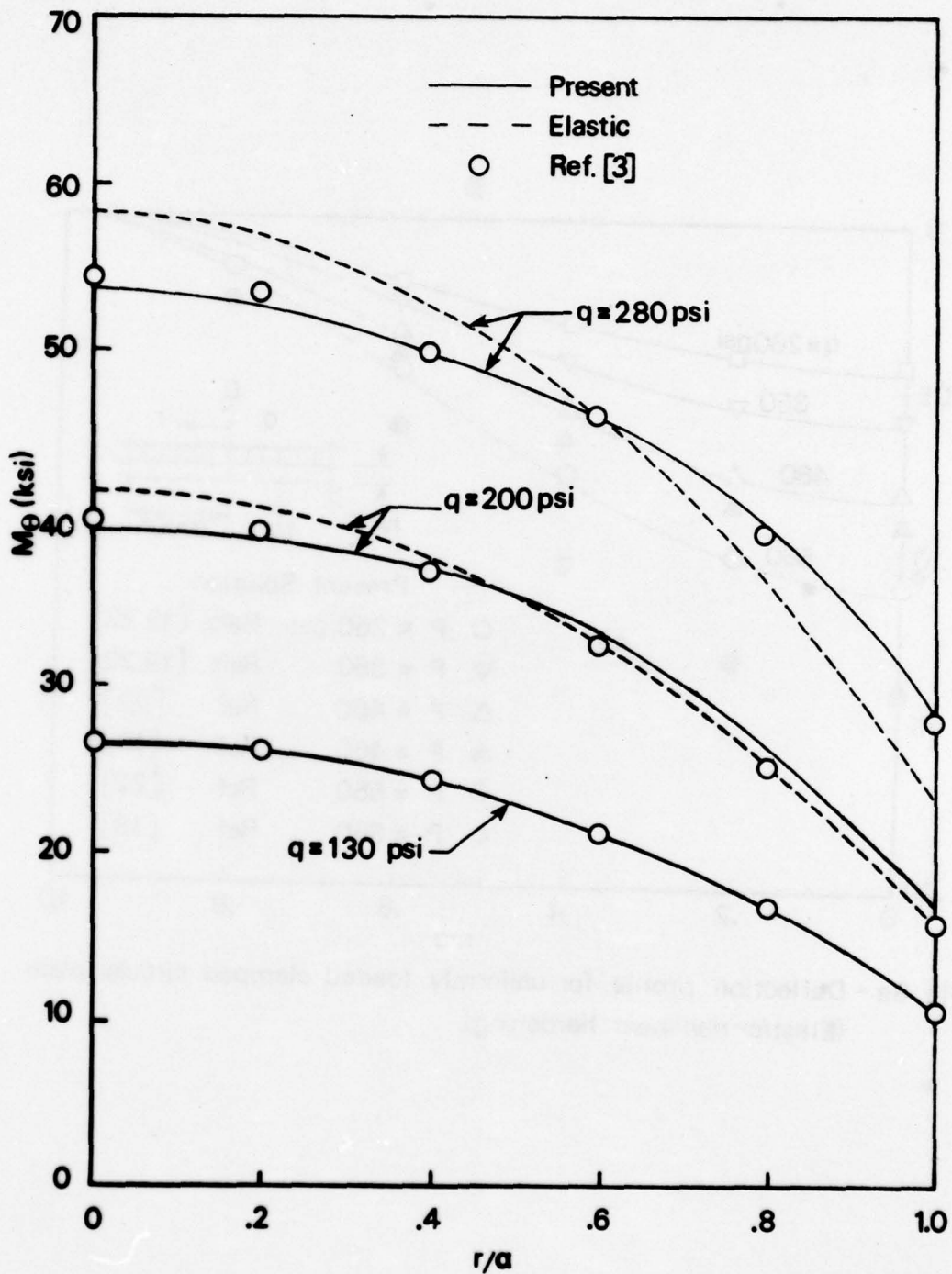


Fig. 7b- Distribution of circumferential moment for uniformly loaded simply supported circular plate (Elastic-linear strain hardening).

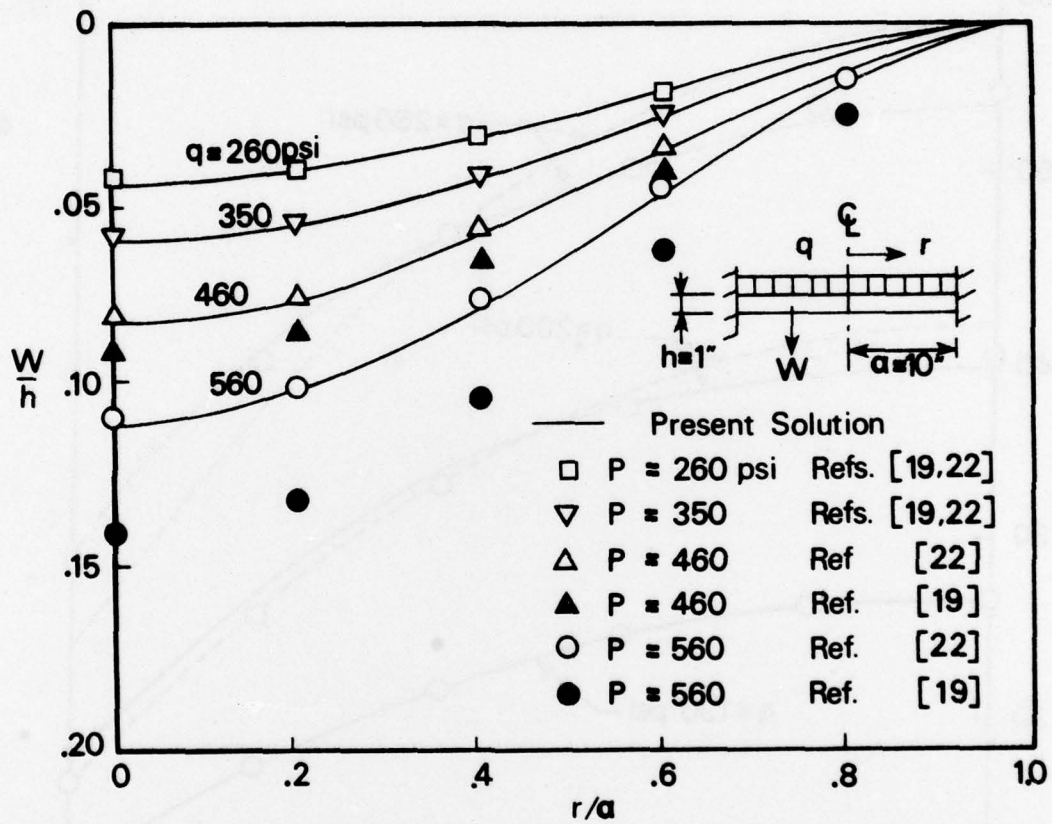


Fig. 8a - Deflection profile for uniformly loaded clamped circular plate (Elastic-nonlinear hardening).

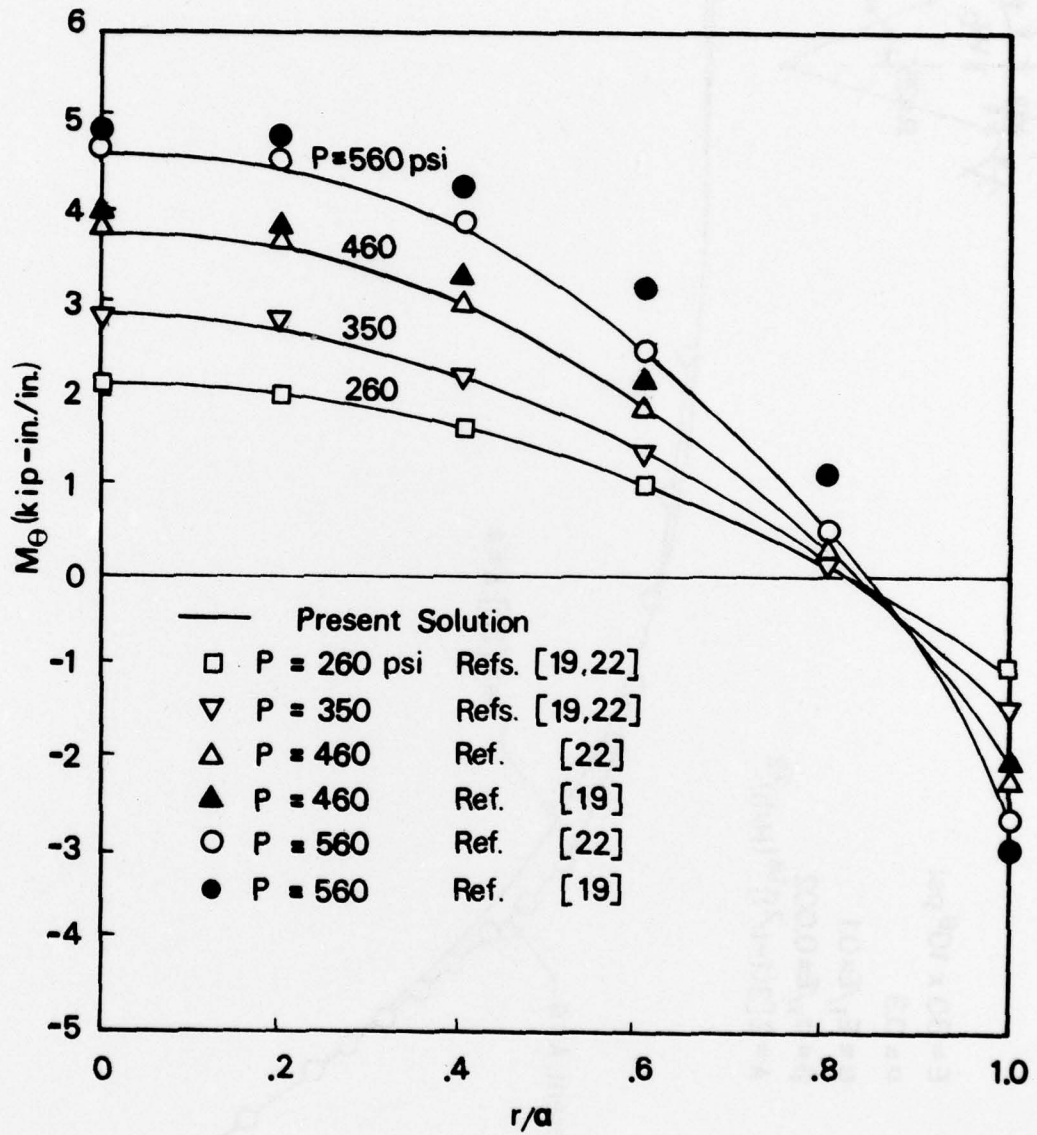
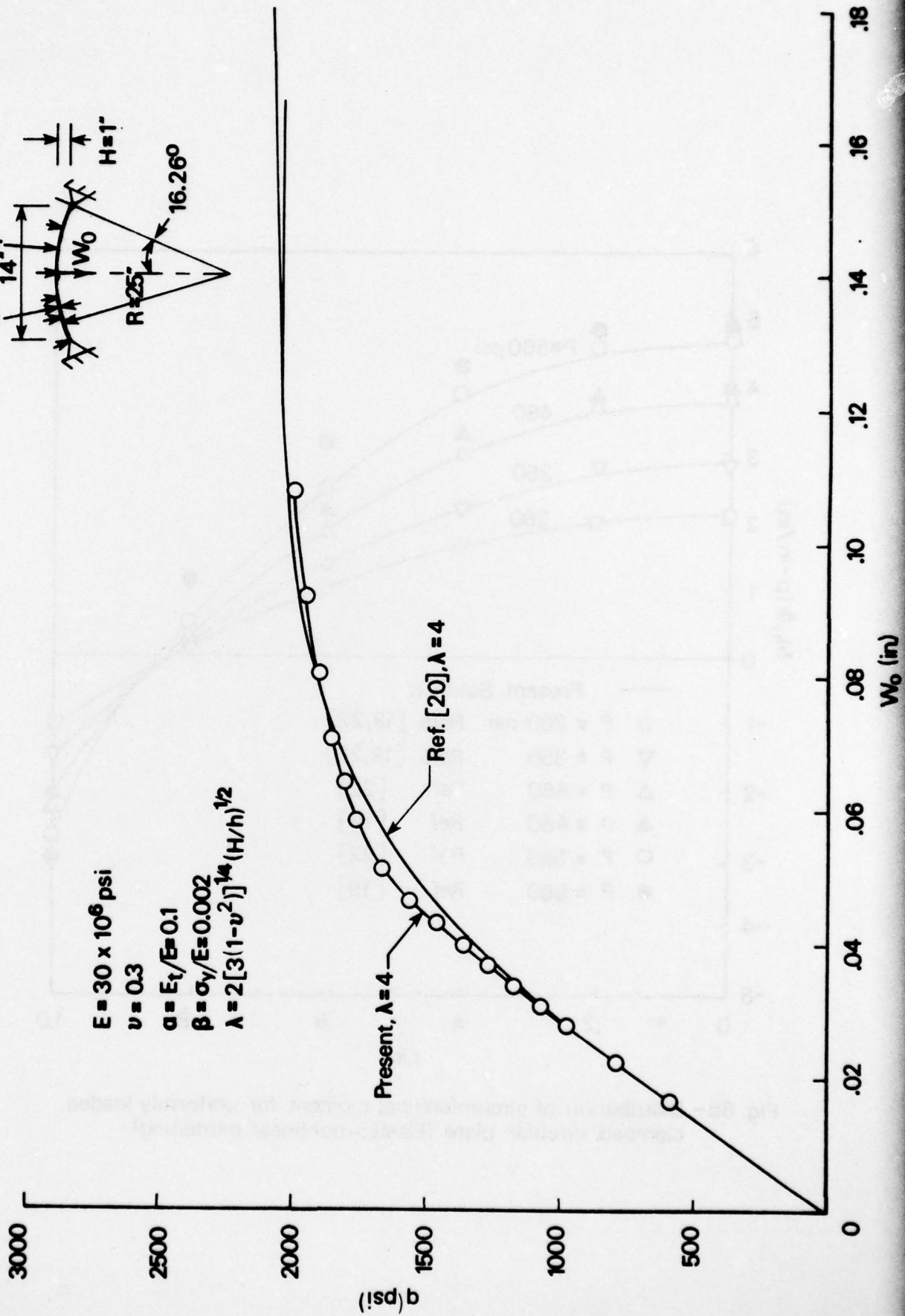
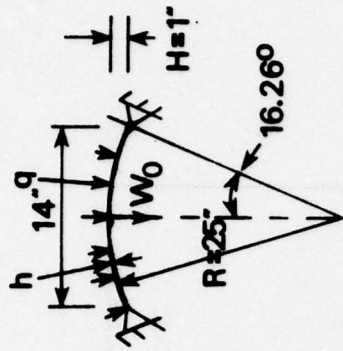


Fig. 8b- Distribution of circumferential moment for uniformly loaded clamped circular plate (Elastic-nonlinear hardening).



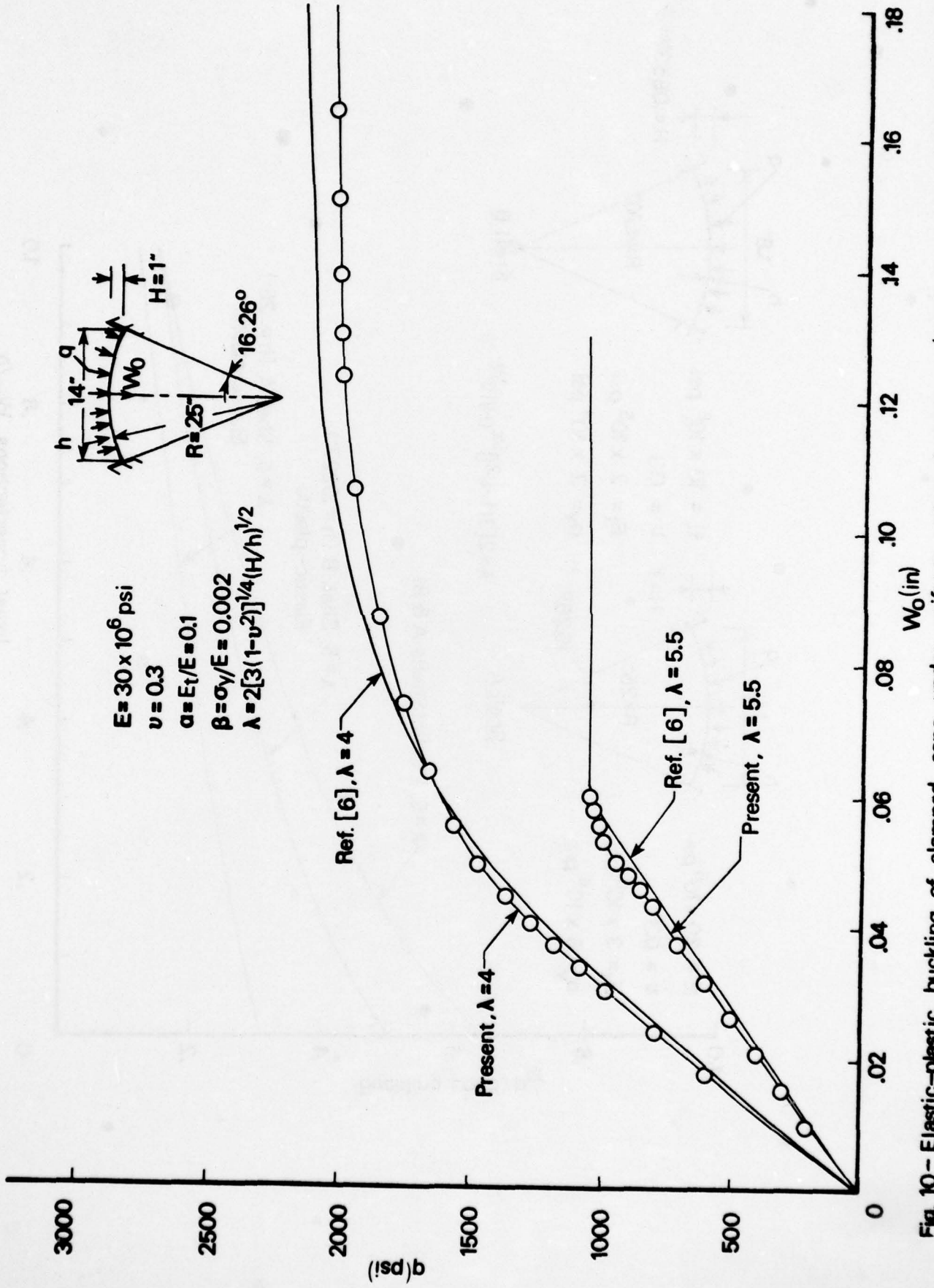
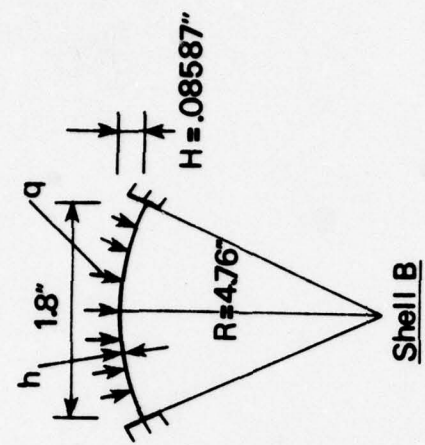


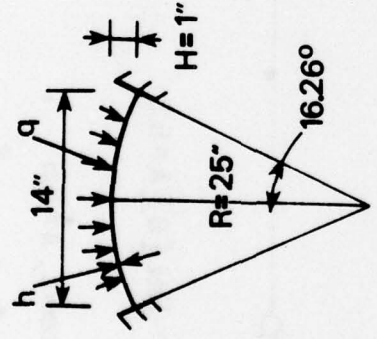
Fig. 10 - Elastic-plastic buckling of clamped caps under uniform external pressure (load vs. central deflection curves).



$E = 30 \times 10^6$ psi
 $\nu = 0.3$
 $E_t = 3 \times 10^6$ psi
 $\sigma_y = 6 \times 10^4$ psi

Shell A

$$\lambda = 2[3(1-\nu^2)]^{1/4} (H/h)^{1/2}$$



$E = 10 \times 10^6$ psi
 $\nu = 0.3$
 $E_t = 2 \times 10^5$ psi
 $\sigma_y = 2 \times 10^4$ psi

Shell B

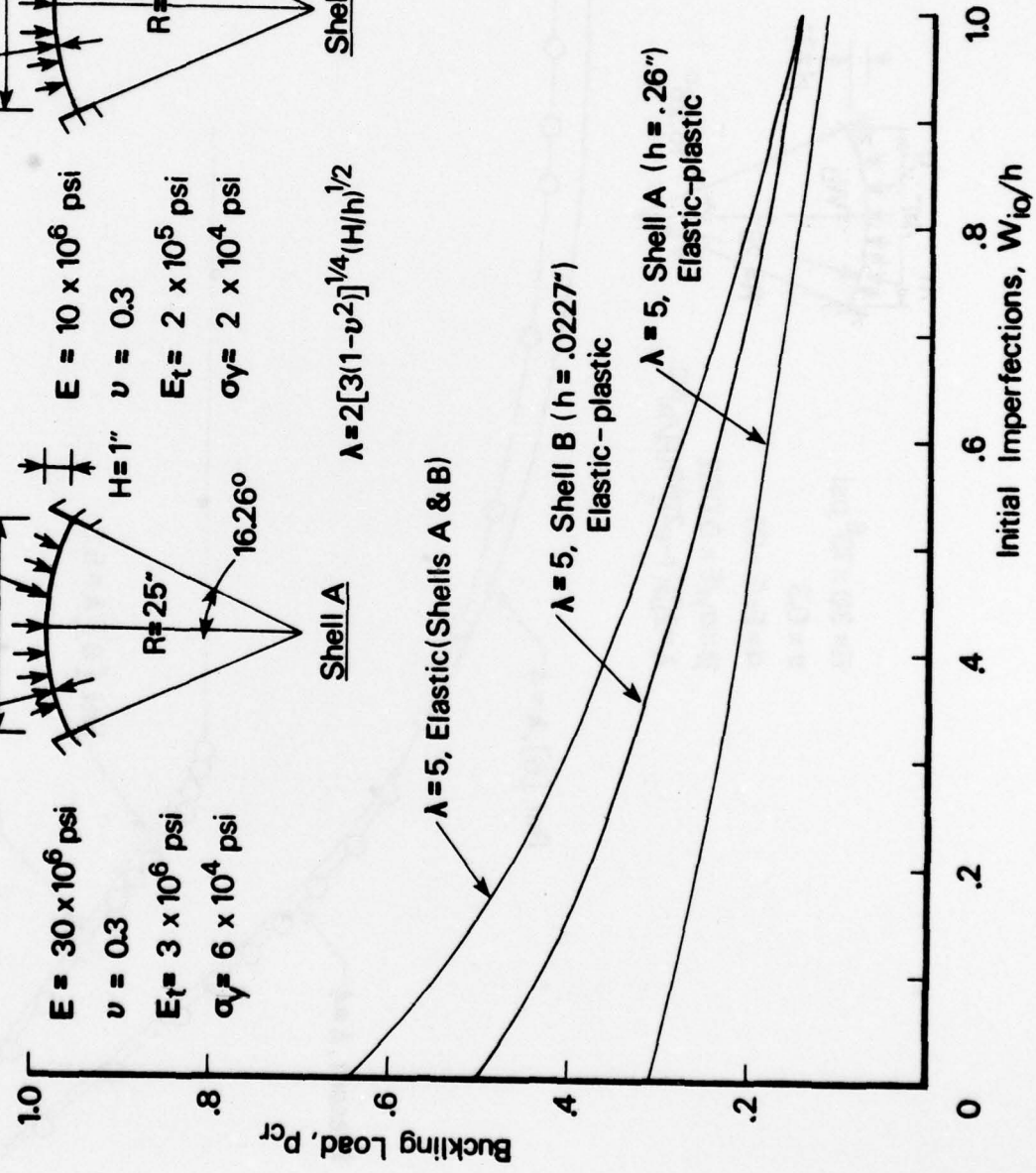


Fig. 17 - Load vs. central lateral deflection for clamped spherical shells. $\nu = 0.3$, $\lambda = 2$, $\mu = 1$, $\sigma_0 = 2$, $\Delta = 1$, $\rho = 1$, $\rho_0 = 1$, $\rho_1 = 1$, $\rho_2 = 1$, $\rho_3 = 1$, $\rho_4 = 1$, $\rho_5 = 1$, $\rho_6 = 1$, $\rho_7 = 1$, $\rho_8 = 1$, $\rho_9 = 1$, $\rho_{10} = 1$, $\rho_{11} = 1$, $\rho_{12} = 1$, $\rho_{13} = 1$, $\rho_{14} = 1$, $\rho_{15} = 1$, $\rho_{16} = 1$, $\rho_{17} = 1$, $\rho_{18} = 1$, $\rho_{19} = 1$, $\rho_{20} = 1$, $\rho_{21} = 1$, $\rho_{22} = 1$, $\rho_{23} = 1$, $\rho_{24} = 1$, $\rho_{25} = 1$, $\rho_{26} = 1$, $\rho_{27} = 1$, $\rho_{28} = 1$, $\rho_{29} = 1$, $\rho_{30} = 1$, $\rho_{31} = 1$, $\rho_{32} = 1$, $\rho_{33} = 1$, $\rho_{34} = 1$, $\rho_{35} = 1$, $\rho_{36} = 1$, $\rho_{37} = 1$, $\rho_{38} = 1$, $\rho_{39} = 1$, $\rho_{40} = 1$, $\rho_{41} = 1$, $\rho_{42} = 1$, $\rho_{43} = 1$, $\rho_{44} = 1$, $\rho_{45} = 1$, $\rho_{46} = 1$, $\rho_{47} = 1$, $\rho_{48} = 1$, $\rho_{49} = 1$, $\rho_{50} = 1$, $\rho_{51} = 1$, $\rho_{52} = 1$, $\rho_{53} = 1$, $\rho_{54} = 1$, $\rho_{55} = 1$, $\rho_{56} = 1$, $\rho_{57} = 1$, $\rho_{58} = 1$, $\rho_{59} = 1$, $\rho_{60} = 1$, $\rho_{61} = 1$, $\rho_{62} = 1$, $\rho_{63} = 1$, $\rho_{64} = 1$, $\rho_{65} = 1$, $\rho_{66} = 1$, $\rho_{67} = 1$, $\rho_{68} = 1$, $\rho_{69} = 1$, $\rho_{70} = 1$, $\rho_{71} = 1$, $\rho_{72} = 1$, $\rho_{73} = 1$, $\rho_{74} = 1$, $\rho_{75} = 1$, $\rho_{76} = 1$, $\rho_{77} = 1$, $\rho_{78} = 1$, $\rho_{79} = 1$, $\rho_{80} = 1$, $\rho_{81} = 1$, $\rho_{82} = 1$, $\rho_{83} = 1$, $\rho_{84} = 1$, $\rho_{85} = 1$, $\rho_{86} = 1$, $\rho_{87} = 1$, $\rho_{88} = 1$, $\rho_{89} = 1$, $\rho_{90} = 1$, $\rho_{91} = 1$, $\rho_{92} = 1$, $\rho_{93} = 1$, $\rho_{94} = 1$, $\rho_{95} = 1$, $\rho_{96} = 1$, $\rho_{97} = 1$, $\rho_{98} = 1$, $\rho_{99} = 1$, $\rho_{100} = 1$.

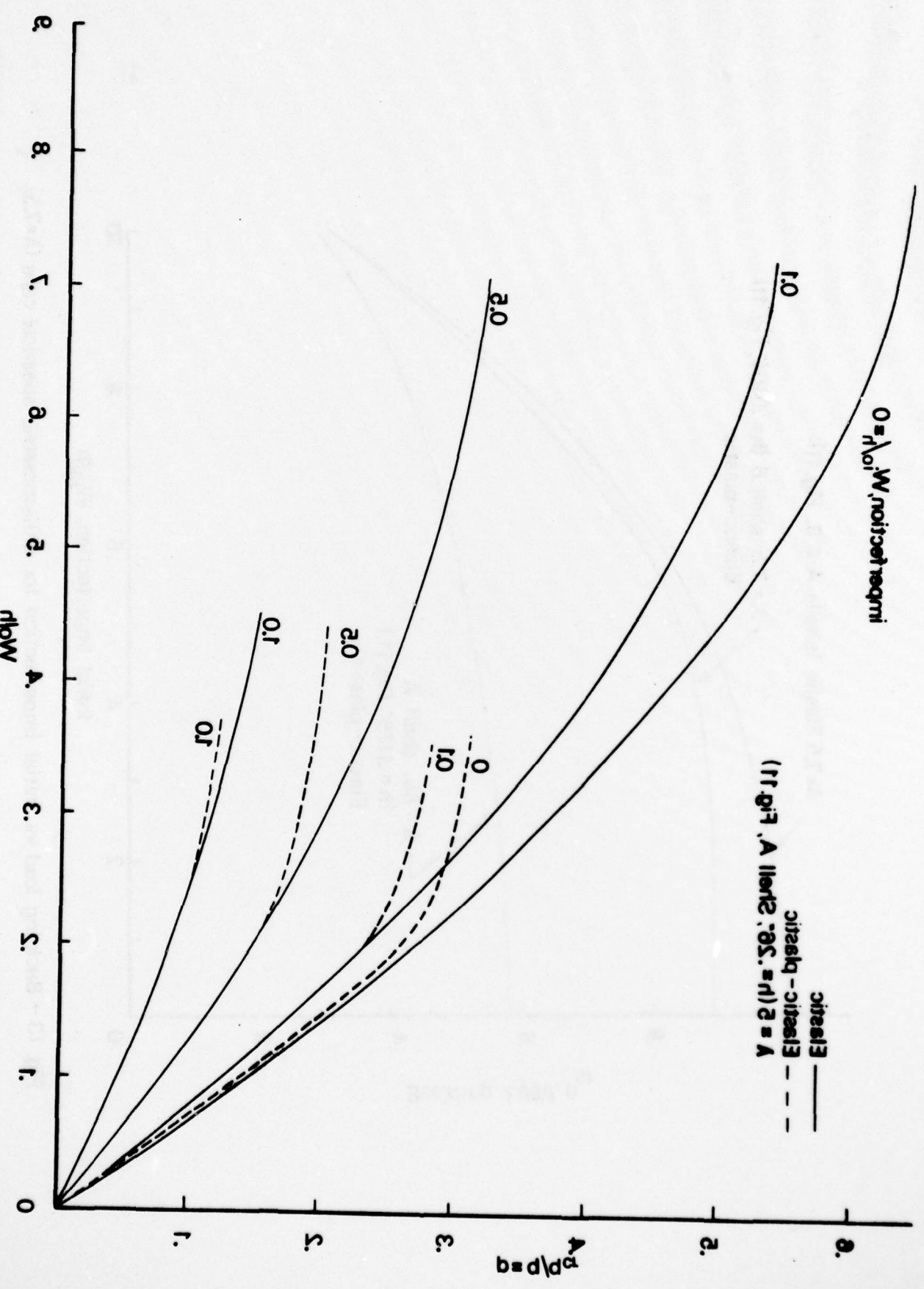


Fig. 17. A shell. $\nu = 0.3$, $\lambda = 2$, $\mu = 1$, $\sigma_0 = 2$, $\Delta = 1$, $\rho = 1$, $\rho_0 = 1$, $\rho_1 = 1$, $\rho_2 = 1$, $\rho_3 = 1$, $\rho_4 = 1$, $\rho_5 = 1$, $\rho_6 = 1$, $\rho_7 = 1$, $\rho_8 = 1$, $\rho_9 = 1$, $\rho_{10} = 1$, $\rho_{11} = 1$, $\rho_{12} = 1$, $\rho_{13} = 1$, $\rho_{14} = 1$, $\rho_{15} = 1$, $\rho_{16} = 1$, $\rho_{17} = 1$, $\rho_{18} = 1$, $\rho_{19} = 1$, $\rho_{20} = 1$, $\rho_{21} = 1$, $\rho_{22} = 1$, $\rho_{23} = 1$, $\rho_{24} = 1$, $\rho_{25} = 1$, $\rho_{26} = 1$, $\rho_{27} = 1$, $\rho_{28} = 1$, $\rho_{29} = 1$, $\rho_{30} = 1$, $\rho_{31} = 1$, $\rho_{32} = 1$, $\rho_{33} = 1$, $\rho_{34} = 1$, $\rho_{35} = 1$, $\rho_{36} = 1$, $\rho_{37} = 1$, $\rho_{38} = 1$, $\rho_{39} = 1$, $\rho_{40} = 1$, $\rho_{41} = 1$, $\rho_{42} = 1$, $\rho_{43} = 1$, $\rho_{44} = 1$, $\rho_{45} = 1$, $\rho_{46} = 1$, $\rho_{47} = 1$, $\rho_{48} = 1$, $\rho_{49} = 1$, $\rho_{50} = 1$, $\rho_{51} = 1$, $\rho_{52} = 1$, $\rho_{53} = 1$, $\rho_{54} = 1$, $\rho_{55} = 1$, $\rho_{56} = 1$, $\rho_{57} = 1$, $\rho_{58} = 1$, $\rho_{59} = 1$, $\rho_{60} = 1$, $\rho_{61} = 1$, $\rho_{62} = 1$, $\rho_{63} = 1$, $\rho_{64} = 1$, $\rho_{65} = 1$, $\rho_{66} = 1$, $\rho_{67} = 1$, $\rho_{68} = 1$, $\rho_{69} = 1$, $\rho_{70} = 1$, $\rho_{71} = 1$, $\rho_{72} = 1$, $\rho_{73} = 1$, $\rho_{74} = 1$, $\rho_{75} = 1$, $\rho_{76} = 1$, $\rho_{77} = 1$, $\rho_{78} = 1$, $\rho_{79} = 1$, $\rho_{80} = 1$, $\rho_{81} = 1$, $\rho_{82} = 1$, $\rho_{83} = 1$, $\rho_{84} = 1$, $\rho_{85} = 1$, $\rho_{86} = 1$, $\rho_{87} = 1$, $\rho_{88} = 1$, $\rho_{89} = 1$, $\rho_{90} = 1$, $\rho_{91} = 1$, $\rho_{92} = 1$, $\rho_{93} = 1$, $\rho_{94} = 1$, $\rho_{95} = 1$, $\rho_{96} = 1$, $\rho_{97} = 1$, $\rho_{98} = 1$, $\rho_{99} = 1$, $\rho_{100} = 1$.

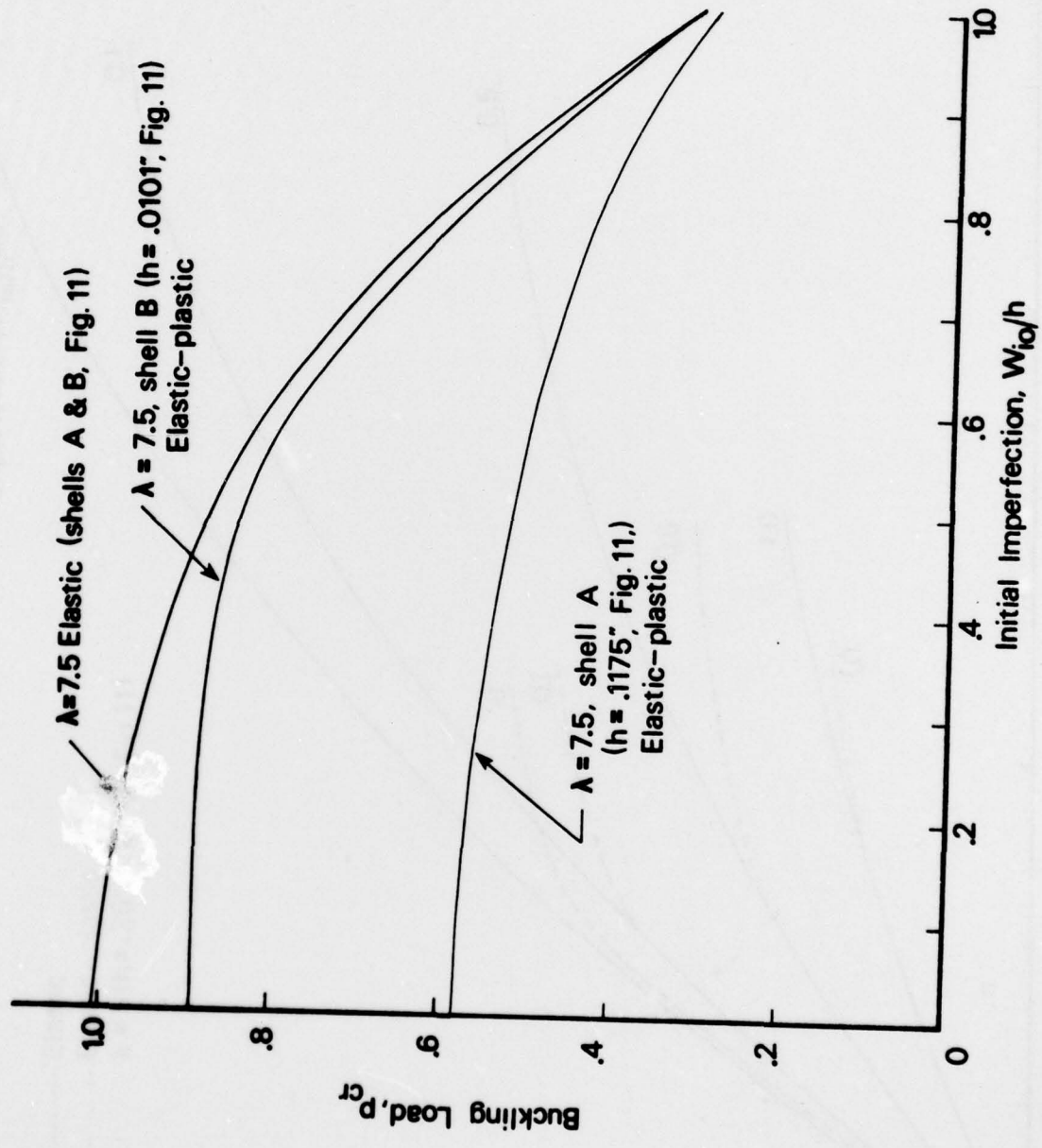


Fig. 13 - Buckling load vs. initial imperfection for axisymmetric spherical caps ($\lambda=7.5$).

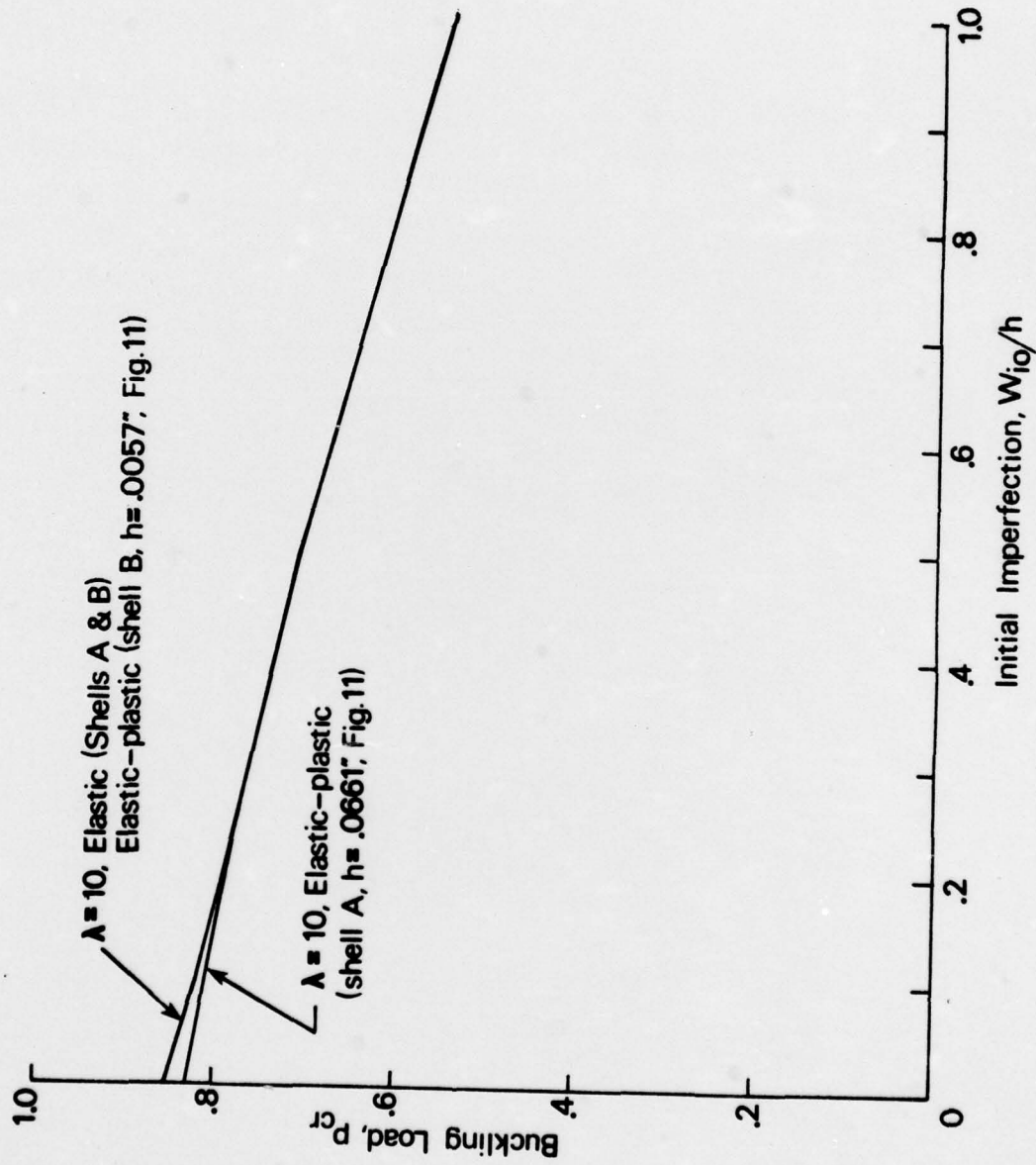


Fig. 14 - Buckling load vs. initial imperfection for axisymmetric spherical caps ($\lambda = 10$).

THE GEORGE WASHINGTON UNIVERSITY

BENEATH THIS PLAQUE
IS BURIED
A VAULT FOR THE FUTURE
IN THE YEAR 2056

THE STORY OF ENGINEERING IN THIS YEAR OF THE PLACING OF THE VAULT AND
ENGINEERING HOPES FOR THE TOMORROWS AS WRITTEN IN THE RECORDS OF THE
FOLLOWING GOVERNMENTAL AND PROFESSIONAL ENGINEERING ORGANIZATIONS AND
THOSE OF THIS GEORGE WASHINGTON UNIVERSITY.

BOARD OF COMMISSIONERS DISTRICT OF COLUMBIA
UNITED STATES ATOMIC ENERGY COMMISSION
DEPARTMENT OF THE ARMY UNITED STATES OF AMERICA
DEPARTMENT OF THE NAVY UNITED STATES OF AMERICA
DEPARTMENT OF THE AIR FORCE UNITED STATES OF AMERICA
NATIONAL ADVISORY COMMITTEE FOR AERONAUTICS
NATIONAL BUREAU OF STANDARDS U.S. DEPARTMENT OF COMMERCE
AMERICAN SOCIETY OF CIVIL ENGINEERS
AMERICAN INSTITUTE OF ELECTRICAL ENGINEERS
THE AMERICAN SOCIETY OF MECHANICAL ENGINEERS
THE SOCIETY OF AMERICAN MILITARY ENGINEERS
AMERICAN INSTITUTE OF MINING & METALLURGICAL ENGINEERS
DISTRICT OF COLUMBIA SOCIETY OF PROFESSIONAL ENGINEERS, INC.
THE INSTITUTE OF RADIO ENGINEERS, INC.
THE CHEMICAL ENGINEERS CLUB OF WASHINGTON
WASHINGTON SOCIETY OF ENGINEERS
FAULKNER KINGSBURY & STENHOUSE - ARCHITECTS
CHARLES H. TOMPKINS COMPANY - BUILDERS
SOCIETY OF WOMEN ENGINEERS
NATIONAL ACADEMY OF SCIENCES, NATIONAL RESEARCH COUNCIL

THE PURPOSE OF THIS VAULT IS INSPIRED BY AND IS DEDICATED TO
CHARLES HOOK TOMPKINS, DOCTOR OF ENGINEERING
BECAUSE OF HIS ENGINEERING CONTRIBUTIONS TO THIS UNIVERSITY, TO HIS
COMMUNITY, TO HIS NATION AND TO OTHER NATIONS.

BY THE GEORGE WASHINGTON UNIVERSITY

ROBERT V. FLEMING
CHAIRMAN OF THE BOARD OF TRUSTEES

GLOYD H. MARVIN
PRESIDENT

JUNE 10, 1956
1956

To cope with the expanding technology, our society must be assured of a continuing supply of rigorously trained and educated engineers. The School of Engineering and Applied Science is completely committed to this objective.